Results from in-beam test runs of a GEM based TPC prototype-noise studies and position resolution in the time direction

L. Bryngemark

Lund University, Lund, Sweden

10.11.2010

Abstract

This Bachelor's dissertation analyses the noise and timing properties of a gas electron multiplier (GEM) based time projection chamber (TPC) prototype, proposed for the International Linear Collider (ILC). The data used are from an in-beam test at DESY (Hamburg, Germany) in February-April 2009. It is found to be a system with low noise and few, if any, systematic spatial correlations of the noise. There is a correlation of noise and pedestal level in read-out channels on certain front end cards (FECs). The drift velocity is $7.60 \pm 0.09\ cm/\mu s$. The time resolution is $10.85 \pm 0.10\ ns$, corresponding to a z direction resolution of $0.7812 \pm 0.0072\ mm$. It is proposed that the FEC dependence of the noise is investigated further, as well as the track width in the z direction. A complimentary computer simulation study is also suggested.

Results from in-beam test runs of a GEM based TPC prototype – noise studies and position resolution in the time direction

Lene Bryngemark

Bachelor's Dissertation

August 2009

LUNDS UNIVERSITET

Abstract

This Bachelor's dissertation analyses the noise and timing properties of a gas electron multiplier (GEM) based time projection chamber (TPC) prototype, proposed for the International Linear Collider (ILC). The data used are from an in-beam test at DESY (Hamburg, Germany) in February-April 2009. It is found to be a system with low noise and few, if any, systematic spatial correlations of the noise. There is a correlation of noise and pedestal level in read-out channel on certain front end cards (FECs). The drift velocity is 7.60 ± 0.09 cm/μs. The time resolution is 10.85 ± 0.10 ns, corresponding to a z direction resolution of 0.7812 ± 0.0072 mm. It is proposed that the FEC dependence of the noise is investigated further, as well as the track width in the z direction. A complimentary computer simulation study is also suggested.

Populärvetenskaplig sammanfattning

Fysikaliska experiment handlar i grund och botten om att undersöka ett orsakssamband på ett sätt som går att registrera. På partikelfysiknivå handlar det om att få partiklar, osynliga för blotta ögat, att ge sig till känna genom växelverkan i detektorer, vilket oftast registreras som en elektrisk signal. Om det går att avgöra var i detektorn den här signalen har sitt ursprung kan ett partikelspår härledas, vilket används för att avgöra vilken partikel som har varit upphov till signalen (det vill säga spåret). Med sådan information kan man till exempel rekonstruera vilka partiklar som har skapats av energin som görs tillgänglig i en partikelkollision.

En TPC (time projection chamber, "tidskammare") är en detektor som kan ge information om en signals ursprung i samtliga tre rumskoordinater. TPCn är en stor gasfylld cylinder med utläsningselektronik i ena änden. En partikel som rör sig genom gasen joniserar gasatomer längs sin väg, det vill säga elektroner från gasen frigörs. De har negativ laddning och rör sig mot pluspolen i ett elektriskt fält. Om det läggs ett lämpligt riktat elektriskt fält över TPCn kommer elektroner, allteftersom de frigörs längs spåret, att driva mot den sida av cylindern där den detekterande ytan och utläsningselektroniken finns. Här kan de, efter förstärkning, registreras som en mycket kortvarig elektrisk ström. Förstärkning av laddningen är nödvändig eftersom en elektrons laddning är för liten för att ge upphov till en mätbar ström.

I den detektorprototyp som studerats här samlas elektronerna upp på anodplattor, ungefär 1×5 mm stora. Förstärkning uppnås genom ett starkt, lokalt elektriskt fält som byggs upp genom hålen på en perforerad platta, GEM (Gas Electron Multiplier), nära anodplattorna. När elektronen befinner sig i fältet (alltså i ett hål) accelereras den och joniserar då gasatomer längs sin väg. De då frigjorda elektronerna kommer i sin tur att jonisera gasatomer, och det blir en lavinförstärkning av laddningen. Till slut har en makroskopiskt mätbar laddning byggts upp. GEMs är ett relativt nytt sätt att åstadkomma förstärkningen – vanligast hittills har varit att använda tunna metalltrådar för att bygga upp det förstärkande elektriska fältet.

Varje anodplatta är kopplad till en utläsningskanal, och plattornas begränsade storlek ger direkt rumskoordinater i två dimensioner för den insamlade laddningen. På hela den detekterande ytan kommer en projektion av partikelns spår att registreras, allteftersom frigjorda elektroner längs spåret anländer. Det är det faktum att det krävs en viss tid för elektronerna att anlända som ger den tredje rumskoordinaten – om de frigjorda elektronernas drifthastighet genom gasen är känd, så kan tidsinformationen från ankomsttiden omvandlas till ett avstånd, och spåret kan nu rekonstrueras i tre dimensioner. Om spåret inte var parallellt med utläsningsplanet, kommer lutningen att synas som en tidsskillnad för ankomsttider längs spåret.

Analysen i den här kandidatuppsatsen använder data insamlade under en testperiod våren 2009, med partikelspår genererade av en elektronstråle på acceleratorlaboratoriet DESY, i Hamburg, Tyskland. Detta var första gången utrustningen användes. Analysen har fokuserat på två områden. Det ena är tidsaspekten av signalerna, såsom drifthastighet, ankomsttid för signaler längs spåret och upplösning i "djupled" (det vill säga tidsdimensionen) i cylindern. Det andra området är signalernas utseende och kvalitet. Här har största vikten lagts vid en analys av brusegenskaper. Den har använt signaler innehållande bara brus, små slumpmässiga variationer i spänningen över kanalerna, som inte är signaler orsakade av partiklar i TPCn utan av omgivande elektronik.

Analysen visar att den här TPCn har mycket lågt brus på signalerna, vilket är önskvärt; i mycket brus kan det vara svårt att skilja ut "äkta" signaler. Bruset tycks vara oberoende av anodplattans position, däremot tycks det finnas en koppling till vilket kretskort (Front End Card, FEC) som hanterar signalen högre upp i datainsamlingshierarkin. Exakt vilka de bakomliggande mekanismerna är behöver studeras ytterligare; det är till exempel oklart om brusnivån är en inneboende egenskap hos varje FEC eller om den är beroende av kortets placering i den större elektronikinfrastrukturen.

Contents

1 Introduction **1**

2 Theoretical considerations **2**
2.1 The International Linear Collider . . . 2
2.2 The time projection chamber . . . 3
2.3 GEM-based read-out . . . 4

3 In-beam test **6**
3.1 The TPC prototype . . . 6
3.1.1 From ionisation track to signal . . . 6
3.1.2 Pad plane geometry . . . 9
3.1.3 Gas mixture . . . 10
3.2 Set-up . . . 10
3.3 Experimental equipment . . . 11
3.3.1 Magnet . . . 11
3.3.2 Chamber gas conditions . . . 11
3.3.3 Beam or cosmic rays? . . . 12
3.3.4 Electronics . . . 12

4 Analysis **14**
4.1 Algorithms . . . 15
4.2 Pedestal runs . . . 17
4.2.1 Noise studies . . . 17
4.2.2 Pedestal studies . . . 19
4.2.3 High gain pedestal runs . . . 21
4.2.4 Causes and correlations of noise and pedestal levels . . . 23
4.2.5 Influence by HV-cables . . . 28
4.2.6 Influence by neighbouring signal cables . . . 28
4.3 Track studies . . . 28
4.3.1 Absolute coordinate corrections . . . 35
4.3.2 Beam angle . . . 35
4.3.3 $\mathbf{E}\times\mathbf{B}$ field effects? . . . 35
4.4 Drift velocity . . . 36
4.5 Resolution in z direction . . . 37
4.5.1 Track width . . . 38

5 Concluding discussion **40**

Acknowledgements **42**

References **43**

Chapter 1

Introduction

In this Bachelor's dissertation, the results of some of the analysis of an in-beam test of a time projection chamber prototype, investigating the performance of a new read-out technology for a detector at the International Linear Collider, are presented. The focus is on the read-out electronics, in particular on noise properties, and on the position given by the arrival time of the electrons from the ionisation of a traversing particle. The main questions asked are:

- What are the characteristics of the noise, and how can they be understood?
- What is the drift velocity in the chamber?
- What is the resolution in the z direction, i.e. the position given by time?

To answer these questions, data from both signals (i.e. collected and amplified charge, released when a charged particle ionises atoms in the detector, measured over a certain time window) and electronic background (noise) is used. Understanding the noise and signal characteristics of a detector is important for setting thresholds and other conditions on arriving signals. Correct settings can reduce the amount of "uninteresting" data recorded. The timing properties are of interest because, firstly, they give the third dimension of a track in this detector type, and secondly the granularity in this dimension (i.e., the sampling frequency) also affects the amount of data handled by the system - and the demand for fast electronics and computing power later in the chain.

First, an introductory background is given which motivates briefly the need for this kind of detector. The detector type is generally described. Then in chapter 3, the in-beam test of the prototype is described, giving more details on this specific prototype and the experimental set-up and conditions. In chapter 4 the results are presented and the algorithms used are explained. Here the results are thourougly discussed as they are presented, focusing on the details. Finally, there is a more general discussion of the analysis, in a broader sense, in chapter 5, which also discusses some topics where further analysis could be done.

Chapter 2

Theoretical considerations

2.1 The International Linear Collider

The field of particle physics right now awaits the start-up of the Large Hadron Collider (LHC) at CERN, in Geneva, Switzerland. In experiments at this accelerator, new physics is expected to be observed, the most well-known probably being the detection of the Higgs particle. There is, however, a difficulty built into the experimental method: hadronic collisions involve the strong interaction in the entrance channel, which is less known than the electromagnetic interaction. Another consideration is that hadrons are composite particles, consisting of *partons*, which implies that the initial energies and states of the interacting partons are poorly known. (However advantageous a spread in energy can be for the purpose of scanning large energy ranges, it is not as good for precision measurements.) This is why a lepton accelerator would be preferrable. But, since the energy loss due to synchrotron radiation is substantial when low mass particles, such as the electron, are accelerated to high energies in a ring, the only way to reach the high energies needed is to use a linear collider. This has to be comparable to the LHC in size, but not much larger, to keep the costs at a reasonable level. This is still very expensive, which makes a joint international effort the only feasible way to realise the plans. All these conditions will be fulfilled in the proposed International Linear Collider (ILC), designed to collide electrons and positrons (see Figure 2.1).

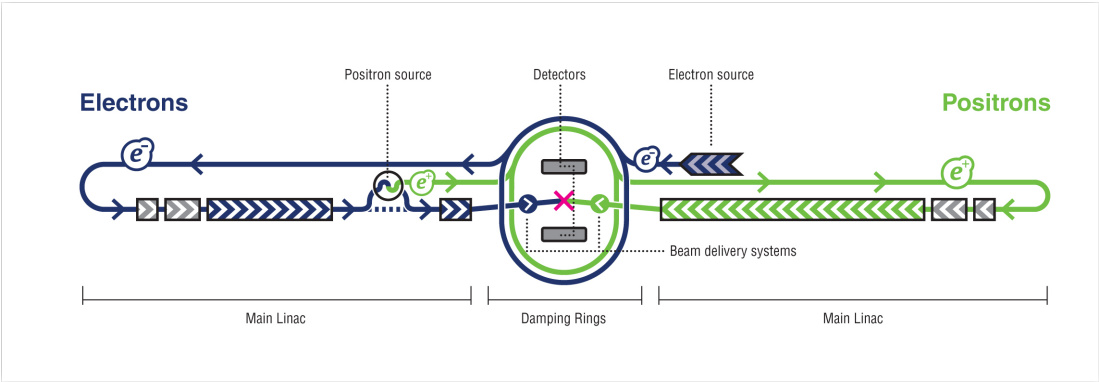

Figure 2.1: Schematic illustration of the proposed linear electron-positron collider design. It's proposed length is 31 km. [8].

The centre-of-mass energy is planned to reach a maximum of 500 GeV, with a foreseen possible upgrade to 1 TeV. This is enough to cover the Higgs boson mass m_H, anticipated from both experimentally set limits and most theoretical considerations (Standard Model and

beyond) to be between 100 and 200 GeV (in natural units). The highest theoretical upper limit of $m_H \leq 700$ GeV would also be covered after the energy upgrade. An integrated luminosity of initially 500 fb^{-1}, and later 1000 fb^{-1}, is expected.

An experiment at the ILC would typically have a tracking system for track reconstruction and momentum determination, a calorimetry system for measuring particle energies and a muon system for identifying and measuring muons. Combining these measurements enables particle identification, both of detected particles and the ones that decayed into them earlier in the chain. Having spatial resolution in the calorimeter, together with a high level of hermeticity greatly enhances the jet resolution and identification of missing energy. The tracking system could be a time projection chamber, which is the type of detector investigated in this analysis.

While the LHC is built to discover new physics, the ILC will be designed to be a precision measurement machine. Many of the interesting new processes are expected to appear in multi-jets. The separation of particle tracks, energies, momenta etc. is thus quite a difficult task. This calls for detectors of unprecendented resolution [1].

2.2 The time projection chamber

The principle of detecting charged particles in a Time Projection Chamber (TPC) is as follows (illustrated in Figure 2.2): the TPC being a gas filled detector implies that an entering charged particle ionises gas atoms along its path. The electrons that are knocked out are caused to drift towards one end of the TPC by an electric field. This end is instrumented with avalanche chambers (providing noise free amplification), followed by read-out electronics.

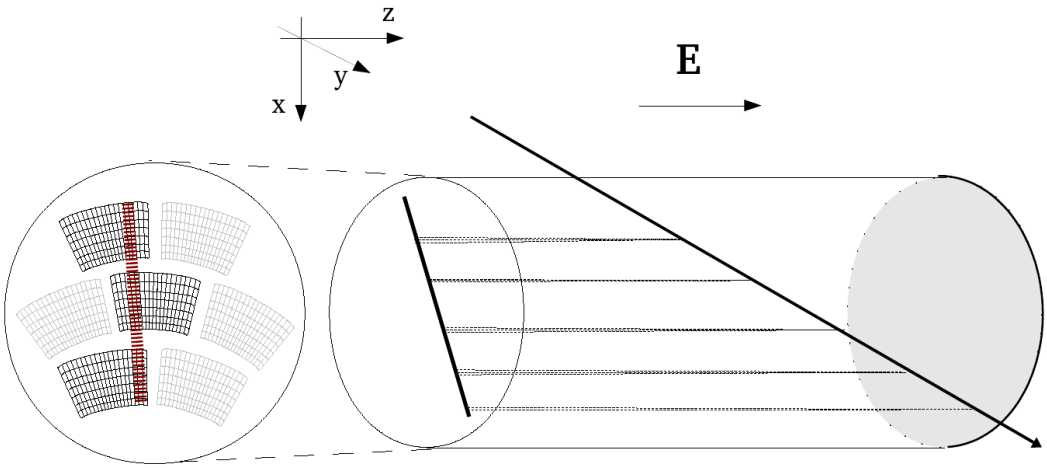

Figure 2.2: The principle of the TPC. A charged particle enters, ionises gas atoms along its track (the tilted arrow) and the released electrons drift toward the field anode, where the charge gives a signal read out on pads. The location of the pad registering the signal gives the track coordinates in the x-y plane. The different arrival times of the signals in pads along the track gives information on the z coordinates. Indicated in the picture is also the coordinate system used in figures to come and an illustration (in red) of a charge from the track collected on the three modules used in the test runs. The grey modules indicate module positions not used.

One of the main reasons for using a TPC for particle detection is its ability to reconstruct particle tracks in three dimensions: two of them given by the coordinates of a signal in a read-out plane (i.e., position of the hit pad), and the third from the arrival time of the signal. Another is that the track is produced with a minimum of influence on the path and energy of the traversing particle, since the medium is a gas.

Traditionally, the TPCs have been of a multi-wire proportional chamber type, meaning that the charge amplifiction necessary for a detectable signal occurs in electric fields emerging from

wires. Close to the wires, the field is increasingly strong, accelerating the electrons towards the wires and causing them to knock out more electrons along their way. This way, an electron avalanche is created, which makes the current large enough for a signal to be detected (either on the wires or on near-by pads). However, in this TPC prototype, no wires are used, but the amplification instead occurs in Gas Electron Multipliers (GEMs) situated just before the read-out pads (see section 2.3).

Using the two spatial coordinates from the pad position in the read-out plane, together with the signal arrival time, it is possible to reconstruct a particle track in three dimensions – call them x, y and *time*. From the drift velocity of electrons in the chamber gas at a given electric field, the *time* coordinate can be translated into a z coordinate.

The main use of the track in a TPC is for momentum determination. For this purpose, a magnetic field parallel to the z axis is applied, which causes the charged particle trajectory to bend in the TPC as the particle traverses it. The bending radius of the trajectory is inversely proportional to the momentum of the particle. Momentum, in turn, is much used for reconstructing the kinematics of a collision and the particles produced (and for particle identification, together with other parameters such as time-of-flight).

The magnetic field also has the big advantage that the diffusion of the drift electrons in the x-y plane is limited to a circle centered on the motion in the z direction of the electron – the drift electron motion towards the read-out plane thus describes a helix. This greatly enhances the resolution in the x-y projection.

2.3 GEM-based read-out

A special feature of this TPC prototype compared to others is the use of GEMs. A GEM is a metal-coated and perforated Kapton foil, typically 50 μm thick, across which an electric field is applied. This gives rise to a local region of high electric field in the holes (as illustrated in Figure 2.3).

The holes are typically of a 70 μm diameter and 140 μm pitch (see Figure 2.4). In these regions, the ionisation electrons accelerate and create an avalanche necessary for a detectable signal. This amplified charge is then collected on the pads, situated a few mm below the GEM, and this charge is the signal from the pad. The two main functions of the wires in a traditional wirechamber - amplifying and collecting the charge - are thus divided between two devices. With several subsequent foils, a considerable amplification can be achieved using a moderate potential difference across each of one them, thus avoiding operation near discharge conditions.[1]

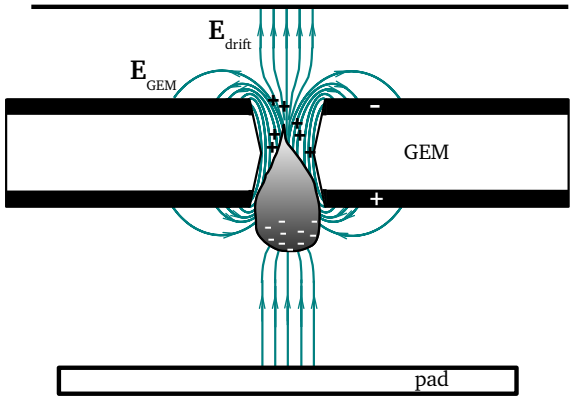

Figure 2.3: Schematic illustration of the principle of amplification in a GEM hole.

One advantage of this amplification method is that it is not the induced signal from the slower moving ions, but rather the collected charge from the electrons themselves that produces the signal. Another one is that the positive ions from the avalanche are to a greater extent than in wirechambers prevented

[1] At a discharge, a gas chamber becomes over-sensitised and its response to incoming charged particles is unreliable. There are often mechanisms to turn off the the high voltage to protect the detector in such cases.

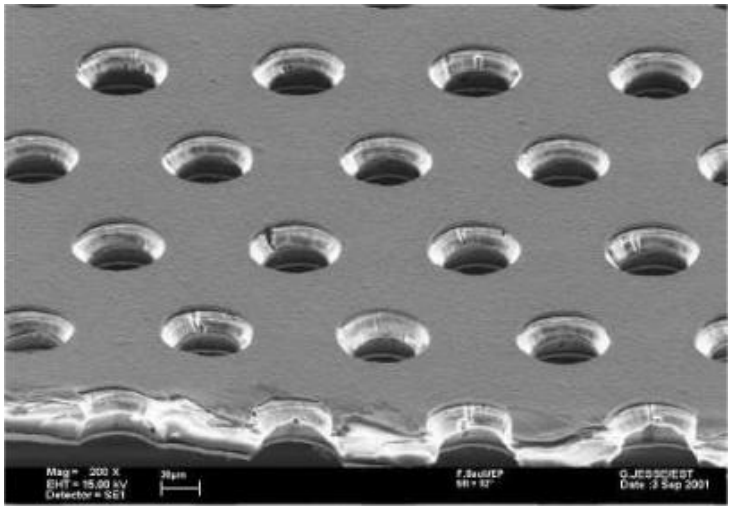

Figure 2.4: Picture of a GEM foil [9].

from drifting backwards into the gas volume (because of the foils) [2]. This gives better gas conditions since positive ions in the gas volume might both distort the electric field and bind track electrons. A third advantage is that the electric field lines after the GEMs are to a larger extent parallel to the magnetic field lines of the TPC, which gives less distorsions from an $\mathbf{E}\times\mathbf{B}$ component.

The major advantage, however, is that using small read-out pads is increasingly difficult with a wire chamber, since the pad dimensions (and distance between pads and wires) have to match the spacing of the wire (if they don't match, the field bceomes too distorted). The risk for discharges increases as the distance gets smaller. As the GEM amplification does not require this geometry matching, the pad size can be much smaller. This enables a better spatial resolution. The hole distance implies that there are several holes above each pad, since these have a size on the order of mm^2.

Chapter 3

In-beam test

This TPC prototype has been built as a joint effort by The international LC-TPC collaboration (where LC stands for linear collider). The first in-beam test was performed at the accelerator facility DESY, in Hamburg, Germany, in Feb-April 2009. The different parts, such as the surrounding magnet, field cage, GEMs and electronics (which will be explained further in section 3.1) were developed by different universities and institutes. The contribution of Lund University (along with Université Libre de Bruxelles and CERN) was the read-out electronics.

3.1 The TPC prototype

3.1.1 From ionisation track to signal

To summarise what was said in Section 2.2: when a charged particle enters the TPC, it ionises the gas along its path. The negative charges released (i.e. electrons) are driven by an electric field towards the pad plane. At a short distance from the pads, there is a charge amplification in the GEM holes, and an avalanche is built up, which is collected in the pad as a signal, proportional to the original charge released in the corresponding portion of the track.

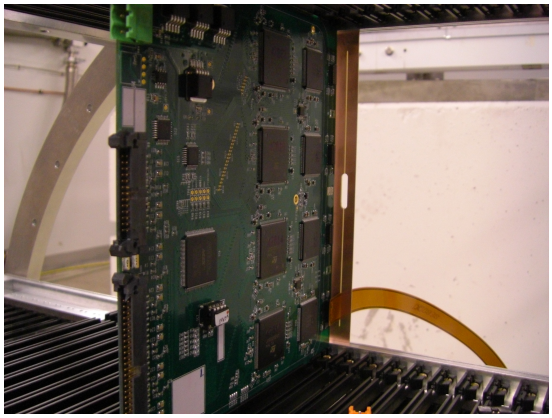

Figure 3.1: An FEC. The 16 signals enter from behind (to the right in the picture) in the signal cable, are preamplified in the PCA16 chip, proceed to the ALTRO chip and are transmitted to the read-out bus through the black connectors in the front (left in the picture).

To collect this charge and convert it to analysable data, the pads are connected to read-out electronics. The read-out chain is roughly: pad - signal cable - Front End Card (FEC) - Read-Out Control Unit (RCU) - data storage.

The electronic set-up is as follows: at each pad there is a connector pin. These are gathered in groups of 16×2 in a connector. Here a signal cable is connected, which carries the 32 signals to two preamplifier shaper chips, named PCA16. An example is seen in Figure 3.2. The PCA16s have 16 channels each, each channel handling one pad, and connections are arranged such that 16 pads in a row in the pad plane are handled by the same PCA16 chip, and the 16 below (or above) are handled by the one on the opposite side of the circuit board. The signal

then reaches the ALTRO (ALice Tpc Read Out) [1] chip, which among other things digitises the signal and buffers signals while waiting for trigger decision on whether to keep the data or not [3]. Each read-out channel is labeled by a (binary) number which gives pin number in ALTRO, ALTRO number in FEC, FEC number in RCU, and finally RCU number.

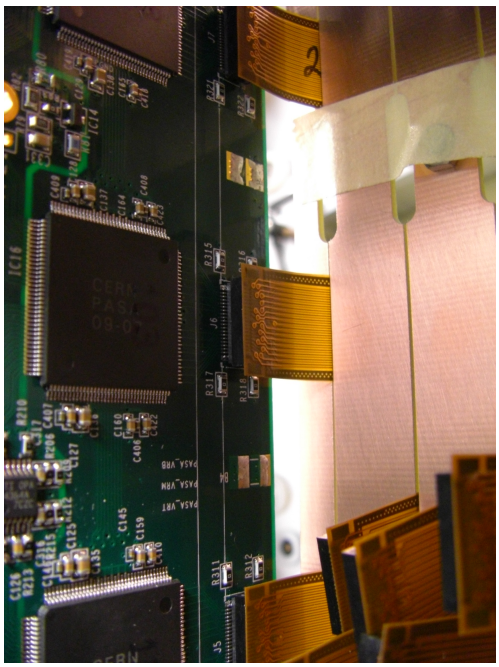

Figure 3.2: Signal cables connected to an FEC. One sees the individual 16 read-out channels on one side of the cable, and the PCA16 that is connected to them. Corresponding read-out channels on the back of the cable are connected to an ALTRO on the opposite side of the FEC.

There are 16 read-out channels per ALTRO, 8 ALTROs per FEC, and a maximum of 32 FECs per RCU. Thus each RCU handles up to 4096 read-out channels. If all the modules installed in this TPC at the test period were instrumented (see Figure 3.9(a)), this would correspond to a total of 15456 read-out channels, requiring 4 RCUs.

The steps of assembling the entire read-out electronics are shown in Figure 3.3.

There is a built-in zero suppression algorithm in the ALTROs, to minimise the load on the RCU and the data transfer and storage capability needed. It simply only allows pulse-like sample sequences to be transmitted to the RCU. The definition of pulse-like can be set with respect to ADC value threshold, number of consecutive samples above this threshold, etc. This is one of the reasons for carefully numbering the individual signals, since an attempt to identify them sequentially would collapse at the first zero-signal, and thus skipped, read-out channel. The possibility to change the zero suppression settings of course brings up the desire to analyse what settings optimise the amount of interesting data with respect to the amount of data that has to be stored.

[1] made by CERN originally for the TPC of the ALICE experiment at LHC

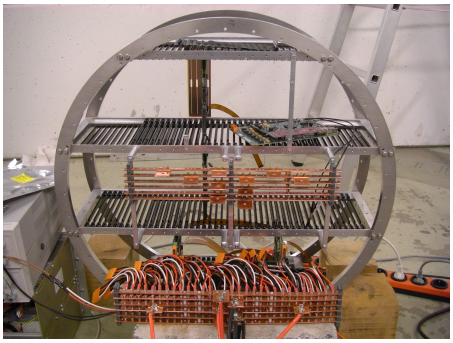

(a) FEC crate

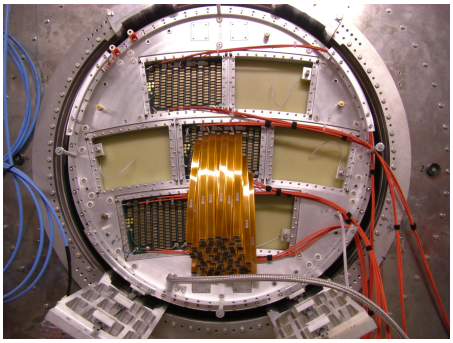

(b) Cables connected to the central module for the 1 module set-up

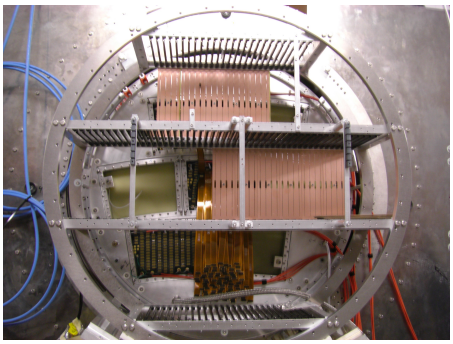

(c) FEC crate in position

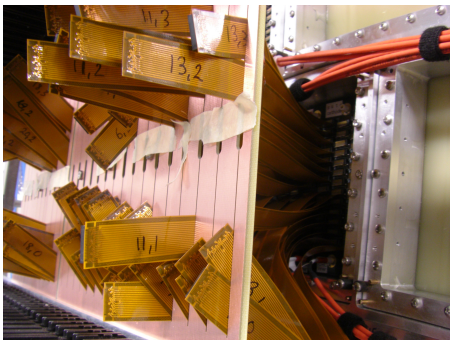

(d) The cables are in position in the slits. The cables are shielded from noise from the electronics by Cu-coated plates

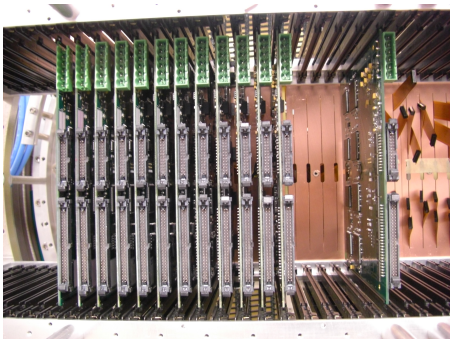

(e) FECs in position

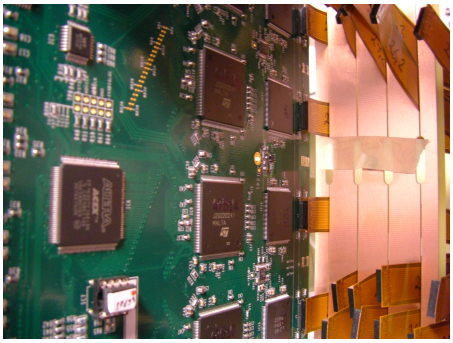

(f) Connection of cables to an FEC

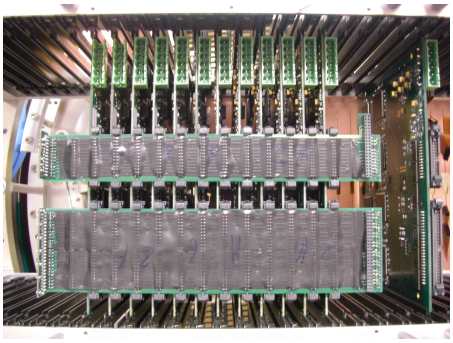

(g) FECs connected to the backplane buses, connecting them to the RCU

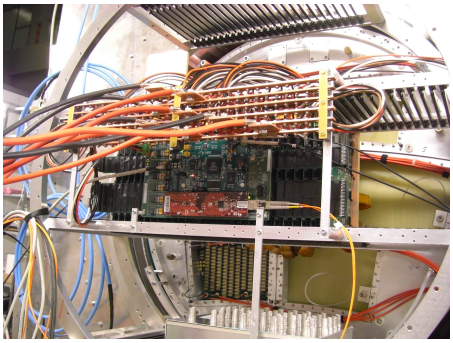

(h) Backplane connected to the RCU, and FECs connected to low voltage supply

Figure 3.3: The steps of connecting the FECs to the pad plane.

3.1.2 Pad plane geometry

The read-out pads are etched on top of a layered circuit board, enabling their traces to reach the cable connector on the back without crossing. The overall geometry of a pad plane module is illustrated in Figure 3.4. The size of a module is roughly 23×15 cm. It resembles a fan, with the pads not being exactly rectangular. The pad rows have a slight arc shape, making up sections of circles, completed by the other modules in a fully instrumented, full-size final TPC. One module has 14×176 pads in the lower half and 14×192 pads in the upper, giving a total of 5152 pads. The transition from 176 to 192 is smooth, implying that the pads get wider from the bottom row up to the middle, and then this repeats itself from the middle to the top of the module. The height, however, is always 5.26 mm. In the figures, the pads will be "lying down" with the height along the x direction. The TPC prototype is prepared to use as many as seven modules; in this test at most three modules were used.

Since this is a more or less circular coordinate geometry with varying pad widths, it is quite hard to represent in a satisfactory way in a two-dimensional histogram figure without using a very large number of bins. Since spatial resolution in x and y is not really the focus of this analysis, no corrections in the translation from module coordinates to absolute pad plane coordinates have been made in the figures, but they are done using the coarse first-attempt mapping provided by the japanese team responsible for the modules and GEMs. The finite resolution binning issue is also what causes many of the white areas that form a regular arc pattern in pedestal run figures to come (see section 4.2).

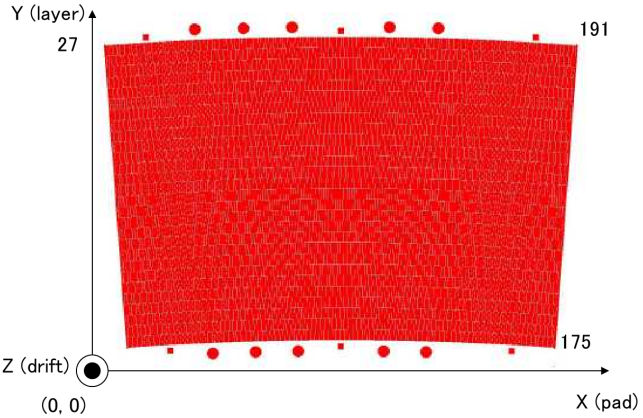

(a) Geometry of a pad plane module. The red circles indicate connectors used for the GEM high voltage etc.

layer #	# of pads	pitch (width, gap)	layer #	# of pads	pitch (width, gap)
13	176	1.25 (1.15, 0.10)	27	192	1.20 (1.10, 0.10)
12	176	1.24 (1.14, 0.10)	26	192	1.20 (1.10, 0.10)
11	176	1.24 (1.14, 0.10)	25	192	1.19 (1.09, 0.10)
10	176	1.23 (1.13, 0.10)	24	192	1.19 (1.09, 0.10)
9	176	1.23 (1.13, 0.10)	23	192	1.19 (1.09, 0.10)
8	176	1.22 (1.12, 0.10)	22	192	1.18 (1.08, 0.10)
7	176	1.22 (1.12, 0.10)	21	192	1.18 (1.08, 0.10)
6	176	1.21 (1.11, 0.10)	20	192	1.17 (1.07, 0.10)
5	176	1.21 (1.11, 0.10)	19	192	1.17 (1.07, 0.10)
4	176	1.20 (1.10, 0.10)	18	192	1.17 (1.07, 0.10)
3	176	1.20 (1.10, 0.10)	17	192	1.16 (1.06, 0.10)
2	176	1.20 (1.10, 0.10)	16	192	1.16 (1.06, 0.10)
1	176	1.19 (1.09, 0.10)	15	192	1.15 (1.05, 0.10)
0	176	1.19 (1.09, 0.10)	14	192	1.15 (1.05, 0.10)

(b) Table showing the widths of the pads for each row

Figure 3.4: Illustration of the geometry of a read-out pad module. All numbers begin with 0. 3.4(a) shows the shape of the module. The x and y directions are interchanged with respect to the coordinate frame used in this analysis. 3.4(b) lists the width of a pad for each row. As the lower 14 rows have fewer pads than the upper half, there is a slow increase in width from the bottom up to the middle, a step at row 14 and another slow increase all the way to the top row. The height is 5.26 mm for all pads, with a gap of 0.1 mm. [10]

The true proportions of the pad width to pad length, which is, as mentioned, varying but roughly 1.2:5.26, is illustrated by a track in Figure 3.5. However, the parameter colour code of the pad, e.g. the charge in the pad, is harder to see than in a figure with both sides of a pad equal. This is the way the pads in the pad plane will be drawn for the three module case, in

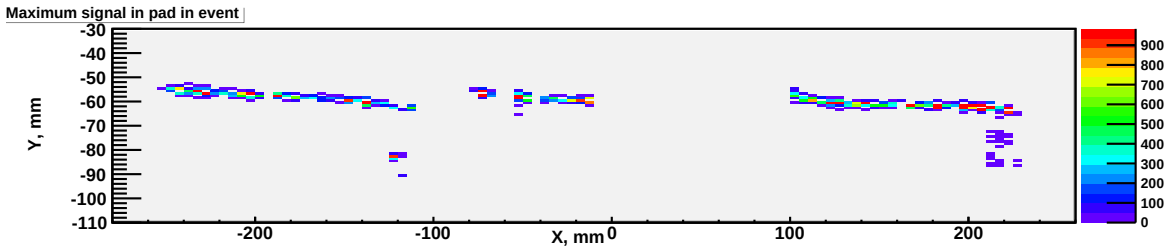

Figure 3.5: True proportions of the pad widths to pad lengths, i.e. perpendicular to and along the beam direction. Note that the three modules are not lined up in a common global coordinate system.

what follows. The real sizes in mm can still be read on the axes.

As is seen from the figure, a track is at most about 50 cm long (using 3 modules). The dimensions of the different instrumented areas can be seen in figures to come (e.g. Figure 4.5(a)).

3.1.3 Gas mixture

The drift volume of this prototype was filled with a gas called T2K [2], consisting of ∼95% argon, and a few percent each of isobutane and freon. This gas is chosen for its very small diffusion, which is favourable for preserving information on the origin of the electron as it drifts.

3.2 Set-up

A schematic view (horisontal intersection) of the experimental set-up is given in Figure 3.6. The TPC cylinder has a radius of 4 dm and is 6 dm deep. The beam is a secondary electron beam from the DESY II accelerator ring. It is generated from pair production as the primary electron beam passes a carbon target and emits bremsstrahlung photons which then produces electron/positron pairs in a metal plate. With a dipole magnet, electrons and positrons are separated and spread out in two horisontal directions and a beam can be chosen using a collimator (as mentioned, the electron beam was used in this experiment). The width of the collimator affects the dispersion and hence the beam angle at the detector. The beam has some energy dispersion from its creation in a target, and one can choose particles of the desired momentum with a dipole magnet. The intensity of the beam at different momenta varies according to the energy distribution of the electrons. The major consideration when choosing the beam energy was for the particles to have enough momentum to accomodate the bend of the trajectory within the rather narrow (∼7 cm) stripe of instrumented pads.

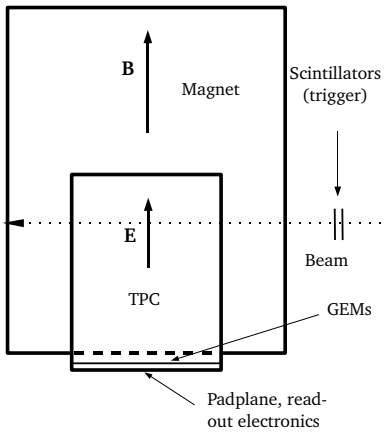

Figure 3.6: Schematic sketch of the set-up; intersection, not to scale. The TPC is drawn inside the magnet. The beam enters from the right, and all figures of particle tracks etc. will be drawn as seen from below in this picture. The position of the trigging scintillators, GEMs, pad plane and read-out electronics are indicated. For a real picture of the TPC and magnet, see Figure 3.8.

The start of a recorded event was set by a trig-

[2] after being used in a japanese neutrino experiment with the same name - acronym for Tokyo To Kamioka

ger, which kept the data acquisition recording data during a certain time window (1000 samples at a sampling rate of 20 MHz, i.e. 50 ns per sample, giving an event length of 50 μs). There was both a trigger for cosmic and for beam events. The scintillators of the beam trigger are depicted in Figure 3.7. The start of an event is marked by a coincident signal in the four scintillators, which should correspond to a beam particle, given the small solid angle covered by both of them.

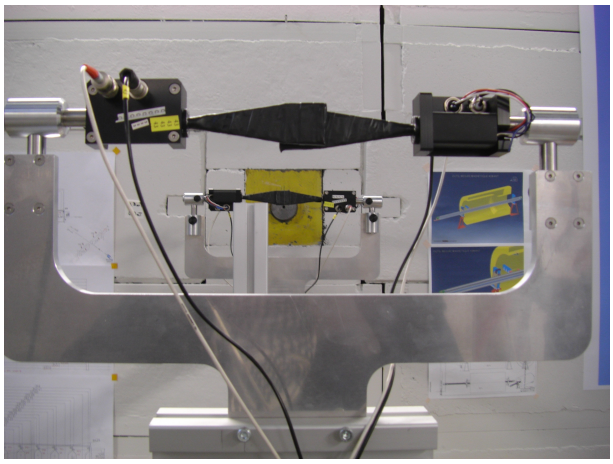

Figure 3.7: The beam trigger uses four scintillators. A coincidence between signals in both pairs should correspond to a beam particle traversing them.

The position of the TPC inside the magnet was varied during the tests, to get different drift lengths of the electrons from the particle tracks – the beam position and the magnet were fixed. This way, the magnetic field conditions in the drift region might have varied slightly for different drift lengths. A moving table, by which the whole magnet and TPC can be moved (enabling a change of both height and transverse position, as well as angle, relative to the beam), was planned but not ready for installation at the time of the test run. It has later been installed [4]. The magnet is described further in section 3.3.1.

3.3 Experimental equipment

3.3.1 Magnet

The magnet was a solenoid with the coil made of superconducting materials, implying the need of cooling to liquid He temperatures. Data was taken with and without magnetic field. The magnetic field was 1 T, not entirely homogeneous (solenoid) field - however, the field at the centre of a solenoid is fairly homogeneous. The magnetic field of the magnet was mapped (for data corrections) by measuring it at different positions with a Hall plate. The field over the length of the TPC in a central positions was homogeneous to within 1% [4]. The magnet was positioned such that the beam traversed here.

Figure 3.8 shows the TPC and the surrounding magnet.

3.3.2 Chamber gas conditions

The pressure and temperature of the chamber gas were measured and logged for every data taking run. These parameters affect the diffusion and drift properties of the gas, avalanche amplification etc. This information can be used for making (small) corrections to e.g. the drift velocity of particles in the gas; however, in this analysis, this is not done.

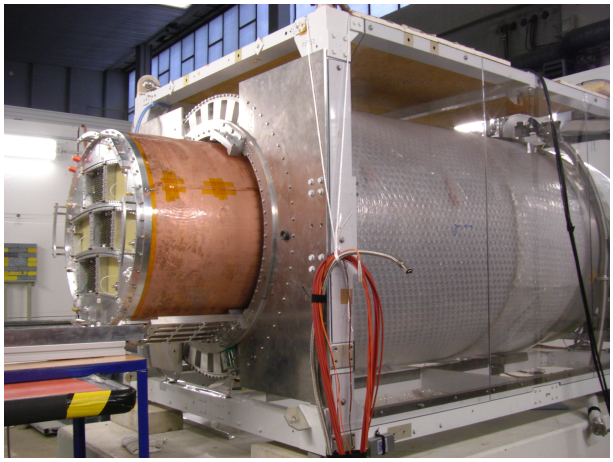

Figure 3.8: The TPC half-way inside the magnet.

3.3.3 Beam or cosmic rays?

Data was taken using both the electron beam and cosmic events. An advantage of the cosmic rays, compared to the beam, is that the entire pad plane and all angles can in principle be covered. This can reveal dead read-out channels, edge effects and such. The obvious disadvantage is that very little is known about the incoming particle, and that they often have a high momentum, giving straight tracks. With a beam, the momentum can be chosen, enabling an analysis of momentum resolution. Also, the rate of hits on the instrumented area is much smaller for cosmics compared to a beam. With the possibility to move the magnet together with the TPC, there is not the same need to use cosmic events.

3.3.4 Electronics

The zero suppression was not fully and reliably operational at the time of the test run. There were runs taken with and without zero suppression, and with different zero suppression thresholds, to make an analysis of this aspect possible – one must of course be certain that using zero suppression does not mean losing interesting data.

Three different cable configurations were used: one instrumenting the central module only, one instrumenting three modules above each other (but only half of the central one, as is seen in Figure 3.9(b)), and finally one instrumenting the entire length of three modules. The latter instrumentation was used in a later test run, when the GEM of the central module had been repaired. Only 26 FECs were available, implying that in none of the cases were modules instrumented fully, and that using one RCU was sufficient. For the three module cases, a narrow band of pads, a few connectors wide, was instrumented in order to cover a full track length.

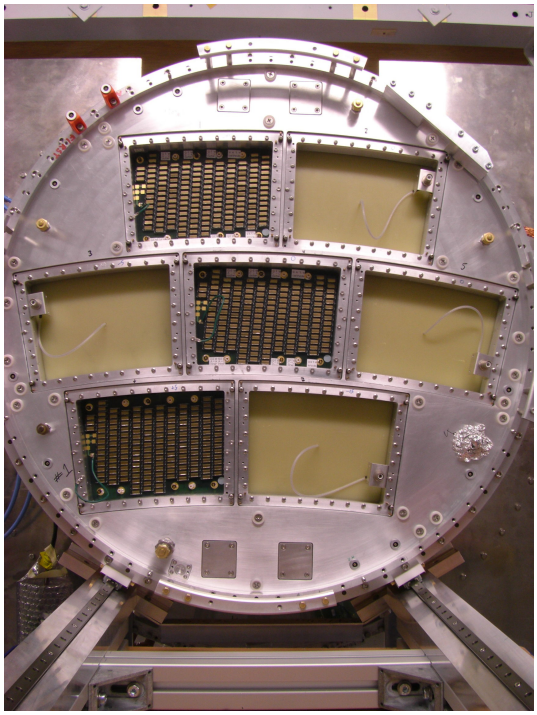

(a) Pad plane connectors

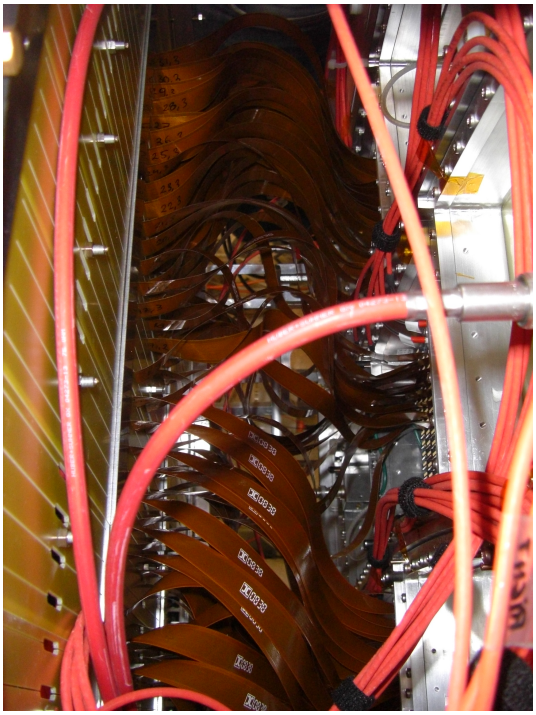

(b) Cables connected to three modules (seen from above). The uninstrumented area in the middle is seen to the right.

Figure 3.9: The TPC is equipped with electronics on three modules. Here the modules are seen uninstrumented (3.9(a)) and fully connected (3.9(b)), with the TPC rotated 90° counter-clockwise compared to Figure 3.9(a).

Chapter 4

Analysis

The main scope of this analysis is properties of the TPC read-out electronics, such as noise levels and timing properties. With these results, further aspects related to the z direction, such as the drift velocity, beam angle etc. are also investigated.

The resolution in the z direction – i.e., the time dimension – depends on the sampling frequency, which was 20 MHz, corresponding to a timesample spacing of 50 ns. A higher sampling frequency should in principle give a better resolution, and 40 MHz sampling frequency will be tested in future experiments [5]. However, there are two reasons why it isn't obviuos that 40 MHz is better. The first is that the transverse momentum of a particle, which is the most important observable, is given by the bending radius in the x-y plane (due to the magnetic field), while the z-dimension of the track remains unaffected by the magnetic field. The second is that the track in, e.g., the x-z plane should be fitted to a first order polynomial, with the first order coefficient only dependent on the track angle with respect to the pad plane. This corresponds to the z direction being measured with a very large number of measurements, and thus a good mean value for this dimension can be obtained, even with poorer resolution in each point. An improved time resolution from a larger sampling frequency, leading to an increased amount of data, might not improve results sufficiently to motivate the additional costs, data volume and power consumption.

The "quality" of the signals, such as noise levels and pulse shape are also investigated. The noise is analysed using what will from now on be referred to as pedestal runs: runs collecting data using a random trigger with beam off, which then do not correspond to a traversing particle. An event in this context is simply the data recorded 1000 timesamples after the trigger has been set off. The pedestal of a read-out channel is the mean signal over time in an event in such a run, and the noise is expressed as deviations from the pedestal in terms of the RMS (the root of the mean of the squared values). In a pedestal run, the pedestal is not subtracted, meaning that the entire information from each read-out channel is stored.

The pulse shape is analysed using beam particle tracks, in zero suppressed data. This aspect also contains information on the optimal settings: a large preamplifier gain might turn out to give saturated signals, i.e. that the signal exceeds the ADC scale used. This factor also affects how coarse the translation from analogue to digital signal is. Each ADC accepts a maximum input of 1.2 V, which is divided into a 1024 channel scale, i.e. roughly 1.2 mV per digital step. Two gain settings are used in this analysis: 12 mV/fC and 27 mV/fC, which will be referred to as low gain and high gain, respectively. As an example, a charge of 1 fC (10^{-15} Coulomb) will with low gain be translated into 10 ADC channels, but with high gain, the same charge corresponds to 23 ADC channels. A higher gain thus gives better "resolution" in the conversion from analogue to digital signal.

It should be kept in mind that amplificion by raising the electronic gain also amplifies the

noise from the environment (electronics and such), while amplification by raising the GEM high voltage is in principle noise free. However, there is a limitation: at too high GEM voltages, sparks may form, causing discharges in the chamber. This is a choice which must be investigated and optimised.

4.1 Algorithms

The algorithms used have been tailormade within the ROOT package (developed at CERN) for this particular analysis. The main analysis algorithm uses an intuitively visual display, showing the pads at their positions in the modules. The analysis takes off from figures where the axes represent the two spatial dimensions of the pad plane, and the parameter analysed is often drawn using a colour scale in the individual pads. Then for a closer look on the time aspect, dependencies and such, other types of visualisations are used. The visual aspect also enters in the feature that one can click on the individual pads in the pad plane figures to (in a separate histogram) see the entire signal in time in that read-out channel, during the event studied.

The main program used does roughly what is described in the flow chart in Figure 4.1.

For the data analysis, a mapping from read-out channel number in ALTRO and FEC to position in the pad plane is necessary. This mapping is stored in files for the different set-ups and looked up by the analysis macro at the beginning of the program execution.

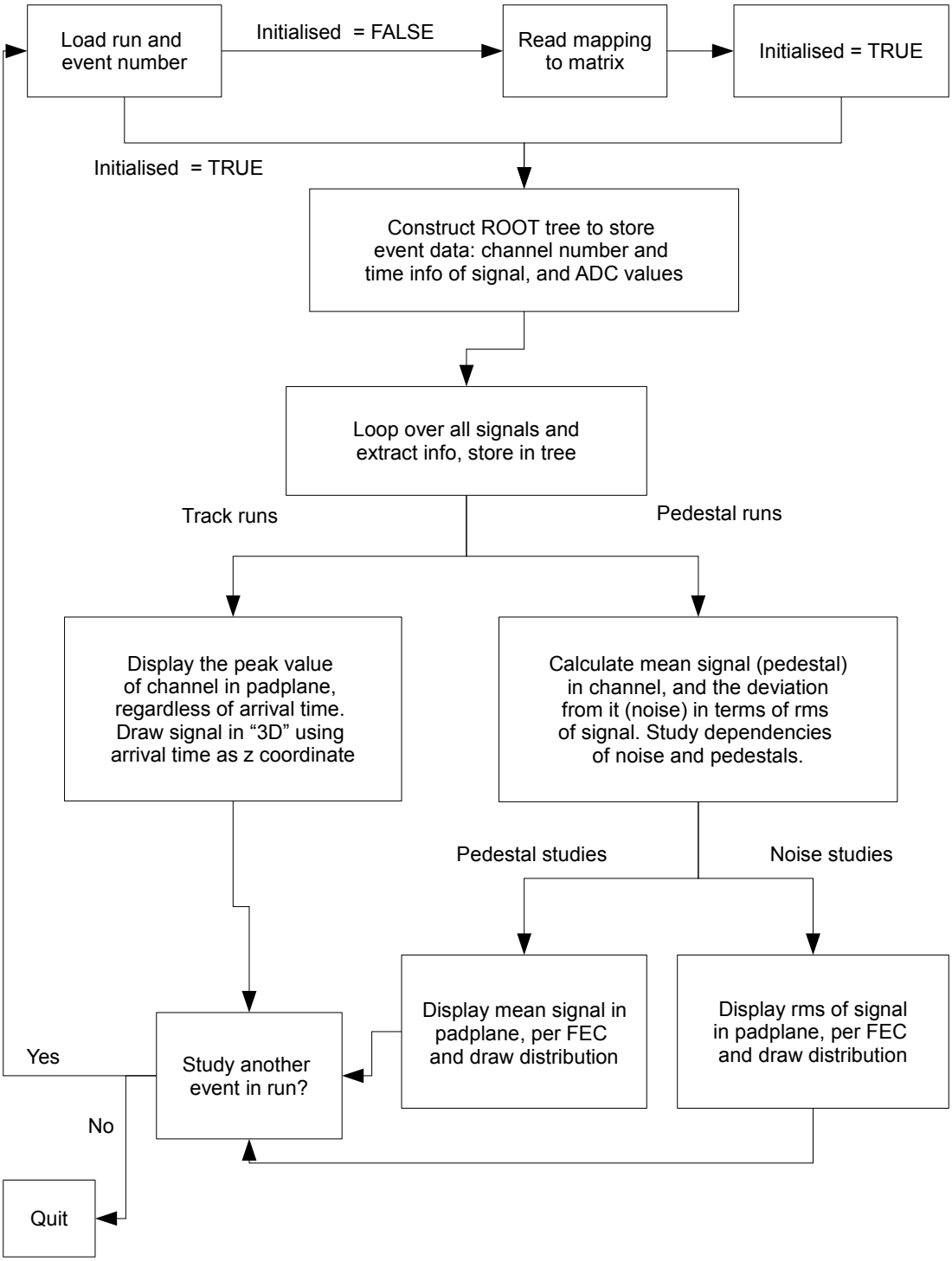

Figure 4.1: Flow chart schematically representing the features and possible choices in the main analysis algorithm, used for an event-by-event signal analysis.

4.2 Pedestal runs

Before cosmic ray and beam runs, some pedestal runs with and without GEM high voltage were performed. The signals in these runs just contain noise from the electronics. It was expected that this TPC would be a low-noise system, even more so since the GEM panels and the electronics are shielded by the TPC cylinder and magnet metal container, much as a Faraday cage. This is indeed the case, as can be seen in figures in the following section. An extra effort has also been made to shield the signal cables from electronic noise, by putting copper coated plates between the FECs and the TPC, and lead the cables through thin slits (as was seen in Figure 3.3(d)).

4.2.1 Noise studies

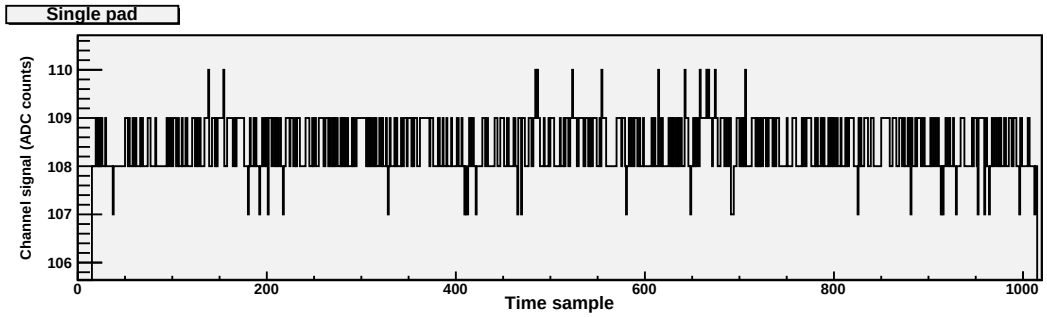

Figure 4.2: A typical signal in one read-out channel during 1000 timesamples of a low-gain pedestal run event. The noise ranges over 3-4 ADC channels, whilst the RMS is typically 0.4 channels. Truncated ADC counts scale.

In a low gain pedestal run, the signal from a read-out channel in an event typically looks like what is shown in Figure 4.2. One event here is simply the entire signal during 1000 timesamples, i.e. 50 μs. Low gain corresponds to 12 mV/fC.

Figures 4.3 and 4.4 show typical low- and high-noise read-out channels, respectively. The low noise is very low; it contains only the random noise from active components in the electronics, such as transistors. The high noise (from external electromagnetic disturbances) will be further discussed later (in section 4.2.4). As will be seen later (section 4.2.4), Figures 4.2 and 4.3 probably correspond to the same noise performance, appearing to be different due to an effect in the finite ADC conversion.

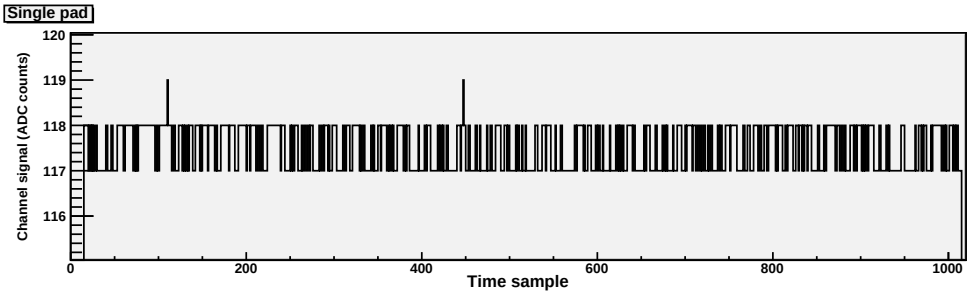

Figure 4.3: A typical low noise signal in one read-out channel during 1000 timesamples of a low-gain pedestal run event. The noise ranges over 2 ADC channels. The ADC counts scale is truncated.

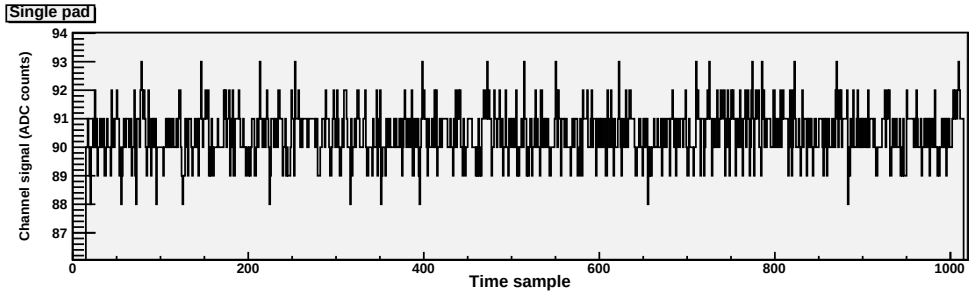

Figure 4.4: A typical high noise signal in one read-out channel during 1000 timesamples of a low-gain pedestal run event. The noise ranges over 6 ADC channels. The ADC counts scale is truncated.

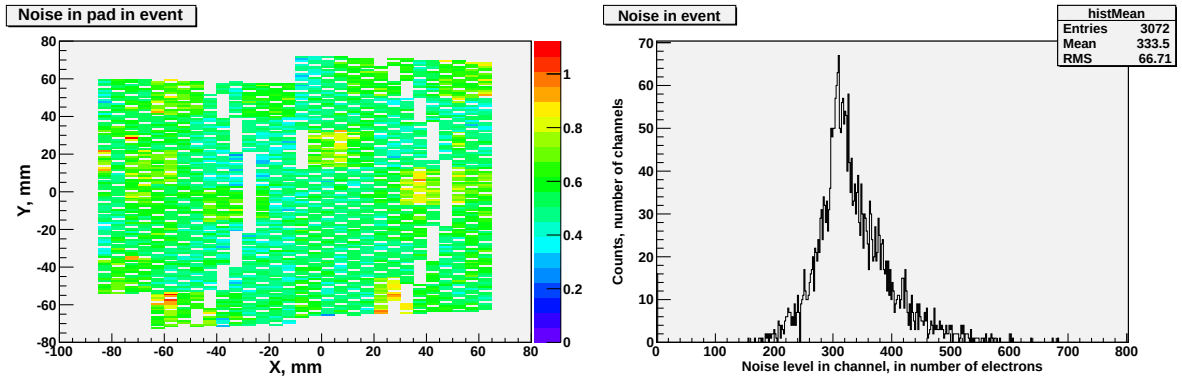

(a) Noise displayed in pad plane coordinates

(b) Distribution

Figure 4.5: Noise, or RMS of pedestal run signal, in all read-out channels in an event. The RMS is calculated from the signal during 1000 timesamples of a low-gain pedestal run event. 4.5(a): Noise in all read-out channels, in ADC values, displayed by colour in the 1 module pad plane of the TPC seen from the back (electronics side). The two white "arches" are a histogram binning effect, due to the somewhat complicated geometry of the module. 4.5(b): Distribution of noise levels in all read-out channels, in number of electrons (converted from fC).

The one module configuration

Figure 4.5(a) shows, in a colour scale[1], the noise levels in ADC values for each read-out channel during one event (which means taking the RMS value of all 1000 timesamples, in pedestal runs), displayed in their pad plane positions. One can discern some groups of higher noise. These correspond to individual signal cables, i.e. as a general trend, the noise levels are fairly uniform within each cable. In Figure 4.5(b), the same distribution of noise level commonly expressed in number of electrons (i.e. number of elementary charges) is histogrammed.

The three module configuration

For use of the beam, 3 modules were partially instrumented. The main reason for not taking beam data using only the central module was that it turned out that only half of its GEM system was fully operational.

Using 3 modules instead of one required a different cabling, and also more FECs were used. There was a slight rearrangement of the FEC positions on the read-out bus. In the figures, FEC number always corresponds to position of FEC on the read-out bus, since this is what assigns the number to the read-out channels. Note also that the numbering of the FECs from left

[1] all colour scales are arbitrarily set to accomodate the lowest and highest values to represent in the event or run

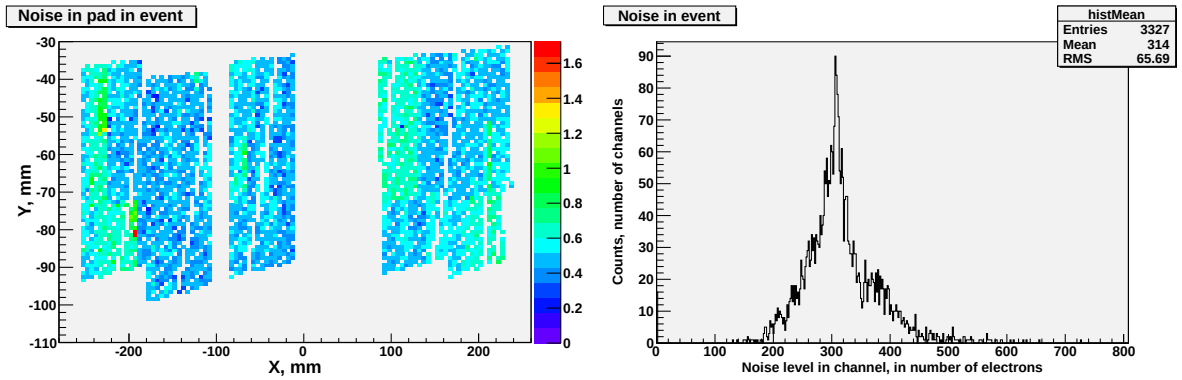

(a) In pad plane coordinates (b) Distribution

Figure 4.6: Noise values in all read-out channels, using 3 modules. 4.6(a): Noise displayed in the 3 module pad plane. Note that the GEM in the right half of the middle module was not operational, and therefore this module not instrumented. 4.6(b): Distribution of noise values in all read-out channels.

to right on the bus is 31-16, 0-15. Thus the FECs are not displayed in the right bus position order in these figures, which should be kept in mind if one attempts to draw any conclusions regarding the physical position of the FECs with respect to one another.

One might wonder if this new cabling results in a different noise. Comparing the noise distribution of the new cabling (Figure 4.6(b)) to that of the former cabling (Figure 4.5(b)), one notices only a slight difference in shape and height. This is discussed further in section 4.2.4.

4.2.2 Pedestal studies

The one module configuration

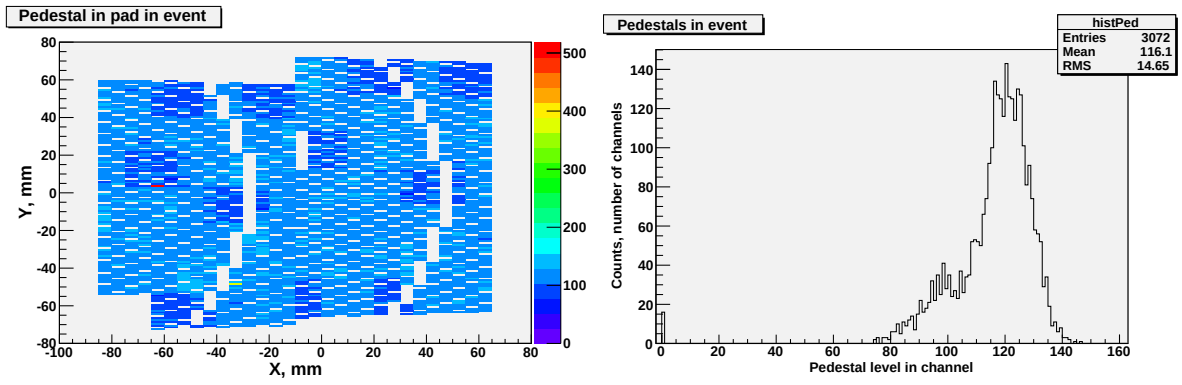

(a) In pad plane coordinates (b) Distribution

Figure 4.7: Pedestal levels in the 1 module, low gain case. 4.7(a): Pedestal levels drawn in pad plane coordinates, colour representing pedestal level in read-out channel. 4.7(b): Distribution of pedestal levels in all read-out channels (highest two not shown). There are 16 "dead" read-out channels in the middle, which have a zero pedestal signal.

There are some general remarks to make about the pedestal levels seen in Figure 4.7(a). Firstly, there are two read-out channels with much higher pedestal levels than the rest (roughly 350 (yellow) and 500 (red), respectively). These are most likely non-functioning read-out channels. Secondly, there seems to be roughly two shades of blue, i.e. two intervals for the pedestal

levels: one at roughly 120 and one somewhere below 100. This is also seen as an extra bump next to the peak in Figure 4.7(b).

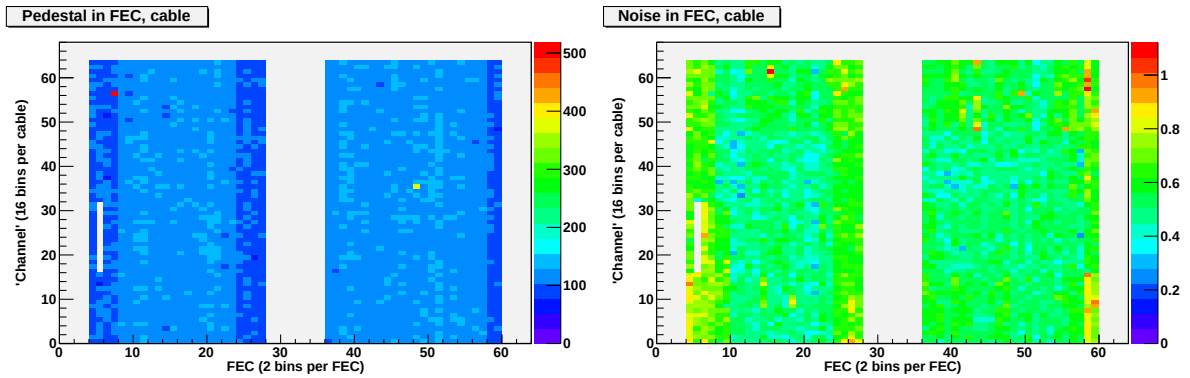

(a) Pedestal levels (b) Noise

Figure 4.8: Distribution of pedestal and noise levels respectively in all read-out channels, drawn per FEC. Note that each FEC is represented by two bins on the horisontal axis (and that the numbering starts at 0). The zero-pedestal read-out channels are clearly seen to the left in both figures.

Figure 4.8(a) shows the pedestal in each read-out channel, displayed per FEC (every FEC is two bins wide, to get the same 16×2 pattern as in the cable connectors. One bin on the x axis thus corresponds to signals handled by one side of the FEC). There is a small but clear difference between individual FECs: FEC 2, 3, 12, 13 and 29 all have generally lower pedestal levels than the rest. They make up the low pedestal bump in Figure 4.7(b) mentioned earlier.

A similar figure is seen in Figure 4.8(b), where instead the noise for the same event is displayed per FEC. One can discern some FEC dependence in the noise, and comparing Figures 4.8(a) and 4.8(b) one sees that FECs with lower pedestals also have higher noise. Additionally, the two lower cables in FEC 4 have a bit higher noise than the rest.

It is clearly seen in the FEC figures, that there are 16 dead read-out channels, i.e. one ALTRO chip which gives no signal at all.

The three module configuration

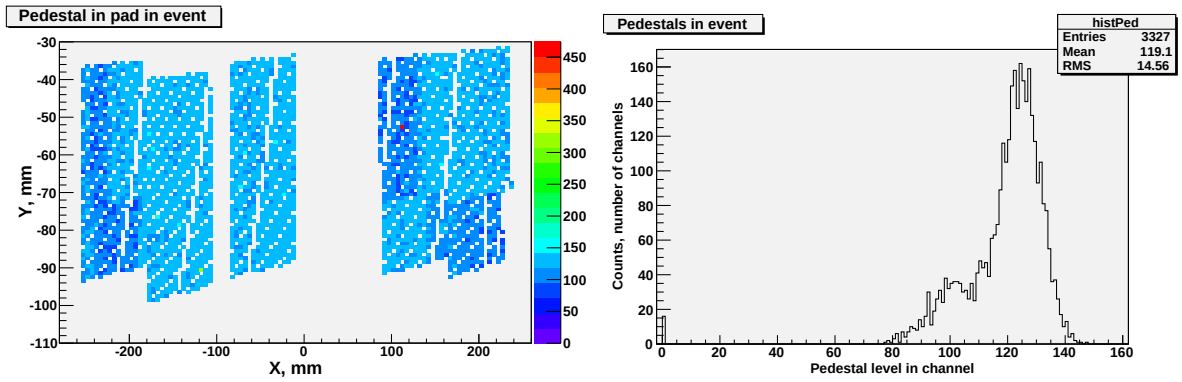

(a) Pedestals in pad plane coordinates (b) Pedestal distribution

Figure 4.9: Pedestal levels for the 3 module, low gain case. 4.9(a): Pad plane display of pedestal levels in displayed in the pad plane. 4.9(b): Distribution of pedestal levels in all read-out channels (highest two not shown).

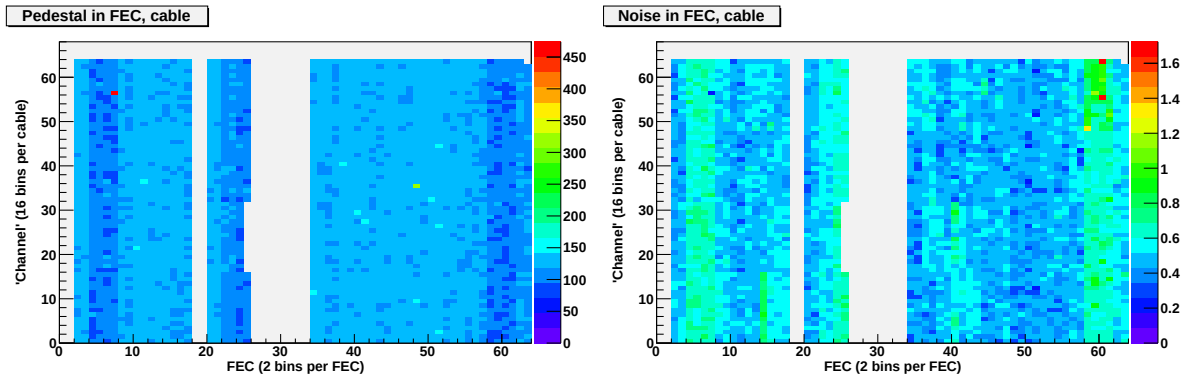

(a) Pedestal levels (b) Noise

Figure 4.10: Pedestal and noise levels respectively in all read-out channels, per FEC, for the 3 module case.

The 3 module, low gain runs display the same behaviour as the 1 module runs, with noise related to FEC, or FEC position on the bus, rather than position in the pad plane. This is to some extent seen in Figure 4.9, but the final ambiguity as to whether this noise has a spatial or FEC dependence is resolved only by Figure 4.10(a). Also in this cabling, there is a correlation between low pedestals and high noise, as can be seen from the comparison of Figures 4.10(a) and 4.10(b).

As the arrangement of the FECs differs between the 1 module and 3 module cases, some FECs are not represented by the same bins any longer, in the figures where e.g. noise is displayed per FEC. Thus some caution should be taken when comparing FEC properties in the 1 module set-up to that with 3 modules, as will be further discussed in section 4.2.4.

4.2.3 High gain pedestal runs

There were also pedestal runs with a higher gain, i.e. larger amplification of the PCA16 signals in the FEC: 27 mV/fC compared to 12 in the low gain runs.

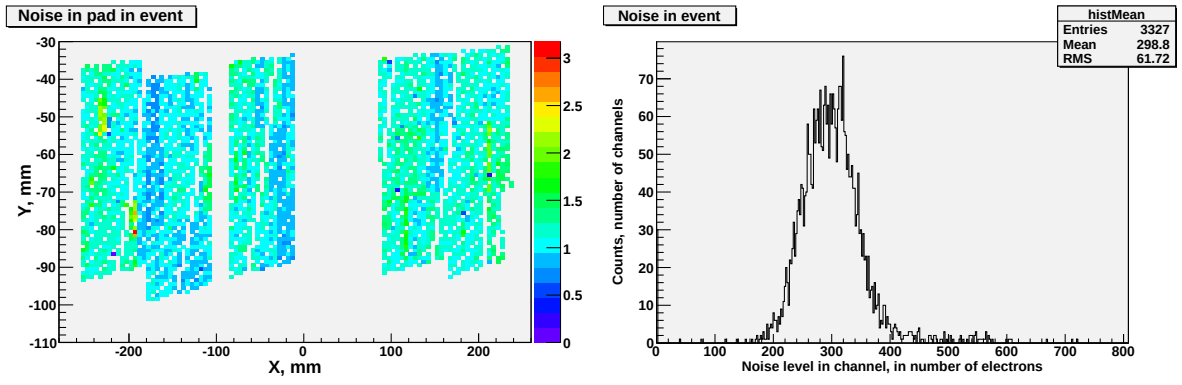

(a) Noise in pad plane coordinates (b) Distribution

Figure 4.11: Noise levels in a high gain run event. 4.11(a): Noise levels in all read-out channels, displayed in pad plane coordinates. Note that the scale is different from the low gain case, as well as the spread. 4.11(b): Distribution of noise levels in all read-out channels. The mean in terms of number of electrons is the same as for low gain runs, but the ADC counts differ due to the different amplification.

The noise figures in Figures 4.11(a) and 4.12 still display some systematics with respect to

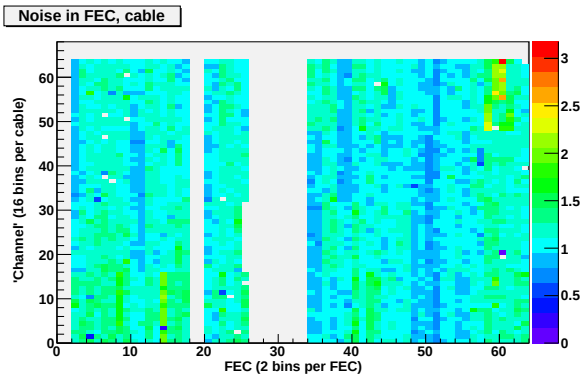

Figure 4.12: Noise levels in all read-out channels, drawn per FEC, for a high gain run event.

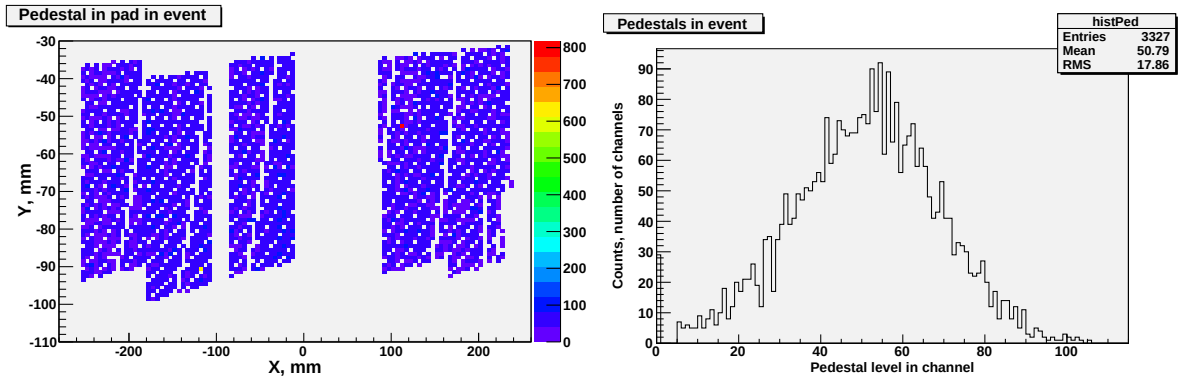

(a) In pad plane coordinates

(b) Pedestal distribution

Figure 4.13: Pedestal levels in a high gain run event. 4.13(a): Pedestal levels in all read-out channels, drawn in pad plane. No clear systematics visible. 4.13(b): Distribution of pedestal levels in all read-out channels (except the highest two), for a high gain run event. There are no bumps as in Figure 4.7(b).

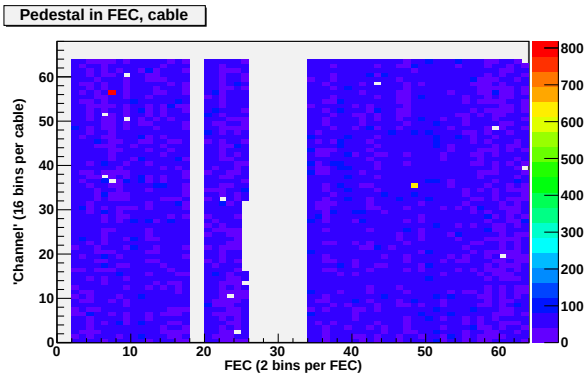

Figure 4.14: Pedestal levels in all read-out channels, drawn per FEC. The previous pattern is gone. There are additional single dead read-out channels apart from the 16 already dead in previous runs.

cables and to some extent FEC position. However, the pedestal levels are much more smoothly distributed in this run than in the low-gain runs, as is seen in Figures 4.13(a) and 4.14. Note that this is not only an impression from a colour scale effect caused by the high pedestal read-

out channels stretching the scale, but the distribution really is smoother too, as can be seen in the distribution in Figure 4.13(b).

4.2.4 Causes and correlations of noise and pedestal levels

One can imagine that the noise would depend on many factors in addition to the intrinsic random noise: pickup effects in the pad plane and signal cables, as well as grounding, differences in the FECs, settings etc. The noise in the 3 module, low gain case (Figure 4.6(a)) at first sight looks as though there are some spatial effects, i.e. more noise at the module boundaries. However, when one draws the noise level in each FEC, there seems to be a much stronger FEC dependence, i.e. the noise levels are fairly homogeneous within each FEC, as has been seen in Figure 4.10(b). Now, one might wonder if this is due to properties of the FECs themselves, or if this effect emerges due to the position on the read-out bus, so moving the FECs to another position on the read-out bus might be desirable.

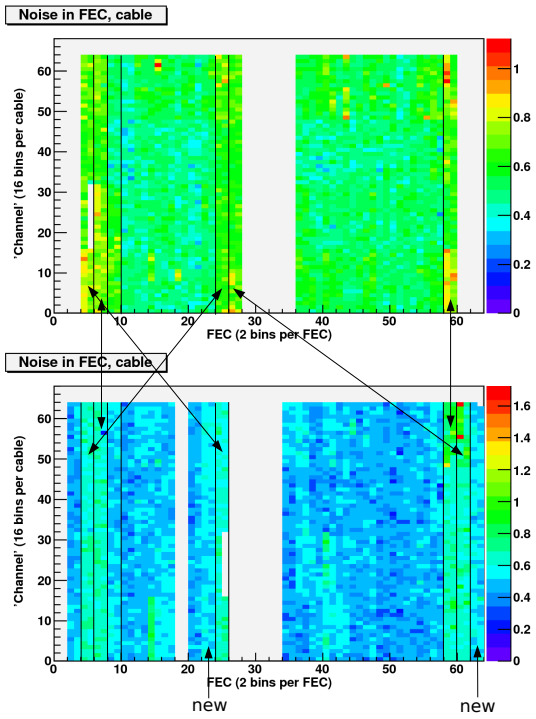

Figure 4.15: Comparison of FEC position on the read-out bus in the 1 module cabling to the 3 module cabling. The noisy FECs that have been moved, have unfortunately switched places. There are two new FECs in the 3 module cabling, which are also a bit noisier than the average.

A comparison between the 1 module and the 3 module set-up, which have slight differences in the FEC positions on the read-out bus (see Figure 4.15), is unfortunately not conclusive as the rearrangement of the FECs was not systematically done, since this effect was not known at the time. It turns out that, in many cases, the FECs displaying the most noise have just switched places.

Thus, the results in this matter remain inconclusive until further investigations are made. The two new FECs in the 3 module cabling were expected to have more noise, from previous tests [5].

Another factor which can affect the noise in a read-out channel is the analogue pedestal

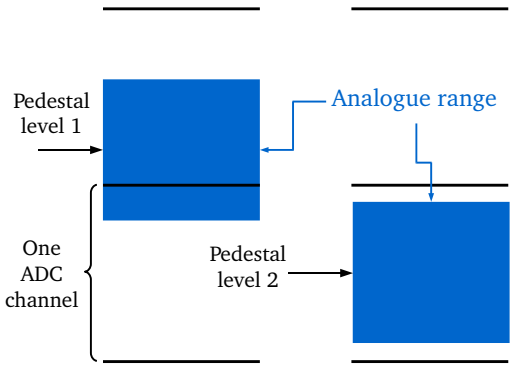

Figure 4.16: This figure illustrates schematically the influence of the position of the analogue pedestal level with respect to the discrete ADC channels. The same range of analogue voltage results in two different ranges of digital values: the interval of pedestal level 1 will span over two ADC channels while that of the other one stays inside the same ADC channel over the entire range of analogue values.

level inside the discrete ADC channel bin, as is illustrated in Figure 4.16. If the analogue pedestal level is close to the edge where the ADC switches to the next discrete channel number, even very small changes in analogue voltage will show. On the other hand, if the pedestal level is centered within the ADC channel, it takes larger differences to change the digital value. This can be tested, since the calculated pedestal levels (averaged over a thousand samples) are generally not integers, while the ADC values are. This effect is in fact clearly visible for the low gain runs, but is not seen for high gain runs, where the noise is amplified and is thus generally spread over several ADC channels. This gain dependence confirms the existence of this effect, and is illustrated in Figure 4.17, which displays noise as a function of the analogue pedestal position inside its digital channel.

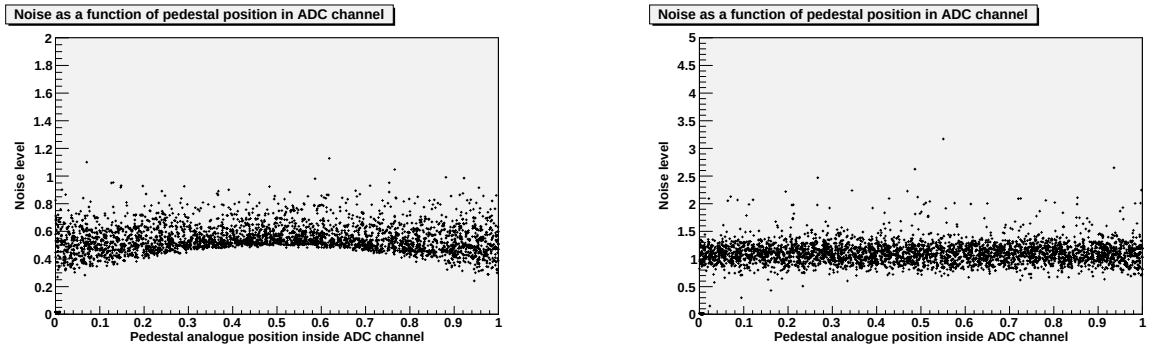

(a) Low gain

(b) High gain

Figure 4.17: 4.17(a): Noise as a function of analogue pedestal position inside the discrete ADC channels (0 = lower limit, 1 = higher limit) in a pedestal run event with low gain. Here is a dependence, visible since the noise generally ranges over only a few channels. 4.17(b): The same figure, but in a run with high gain. Clearly, the dependence is gone, since the sample voltages are spread over more channels.

In low gain runs, the FEC:s that have a low pedestal level seem to have a higher noise. The dependence of noise on pedestal level is investigated in Figure 4.18(a). The figure shows two "islands" of noise levels, much in the same way as there are two groups of pedestal levels (seen

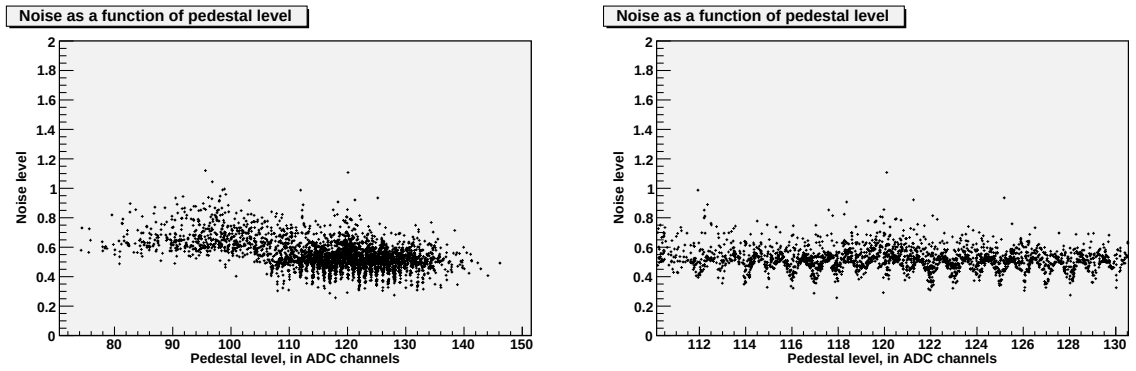

(a) Noise as a function of pedestal (b) Zoom-in on the high pedestal region

Figure 4.18: 4.18(a) shows noise as a function of pedestal in a low-gain run event. The dependence is weak, but there seems to be more or less two regions of constant noise levels. No digitisation effect is seen in the higher-noise region. 4.18(b) gives a closer look at the high pedestal region. The same effect as in Figure 4.17(a) is seen, but now for each integer pedestal interval.

previously in Figure 4.7(b)). Once again, the connection between low pedestals and high noise is clearly seen – however, this dependence is obviously not e.g. linear.

The sawtooth pattern in Figure 4.18(b) shows the same digitisation effect as the one shown in Figure 4.17(a), but for the individual ADC channels. Note that the noise in itself does not depend on the pedestal level inside the ADC channel, while the *measured noise* does.

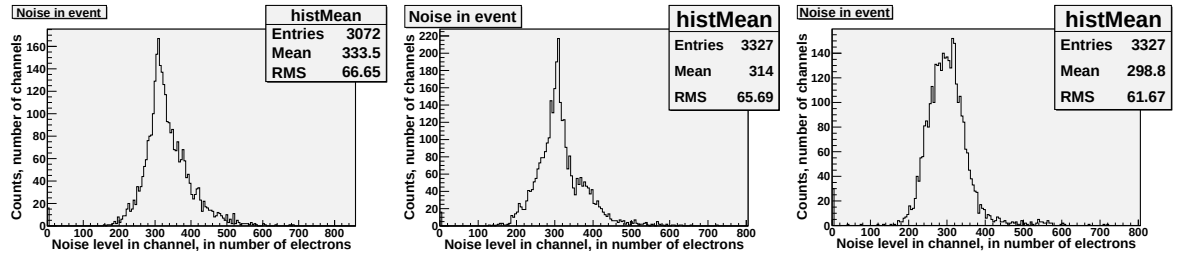

(a) Low gain, 1 module (b) Low gain, 3 modules (c) High gain, 3 modules

Figure 4.19: Comparison of the noise distribution in the three different cases previously discussed (note slightly different count scales): low gain in 1 and 3 modules respectively, and high gain in 3 modules.

Figure 4.19 compares the noise distributions of three different cases: low gain run events with 1 module (4.19(a)) and 3 modules (4.19(b)) instrumented respectively, and a high gain run event with 3 modules (4.19(c)). One sees the slight difference in height and width for the different cablings with the same gain (Figures 4.19(a) and 4.19(b)). Clearly, the noise in terms of absolute charge is more or less constant in the different runs, but the shape of the distribution differs much. Another clear effect is that the the distribution is the broadest in the low gain, 1 module case (4.19(a)), and the narrowest in the high gain, 3 module figure (4.19(c)). In the low gain cases, some of the spread is due to the digitisation effect. In these runs, as has become clear in this section, not all the noise is visible: the low noise is suppressed by the digitisation effect when the analogue signal only changes within the same digital channel. This should explain why the mean is higher and shape much different for these two distributions compared to the high gain distribution of 4.19(c), where the low-noise side is catching up and the distribution is beginning to look more gaussian. As a side remark to this, figures similar to Figure 4.18(a) for

high-gain runs show an even cigar-shaped distribution, which can already be guessed from the distribution in Figure 4.19(c) (being the projection on the noise axis of such a figure).

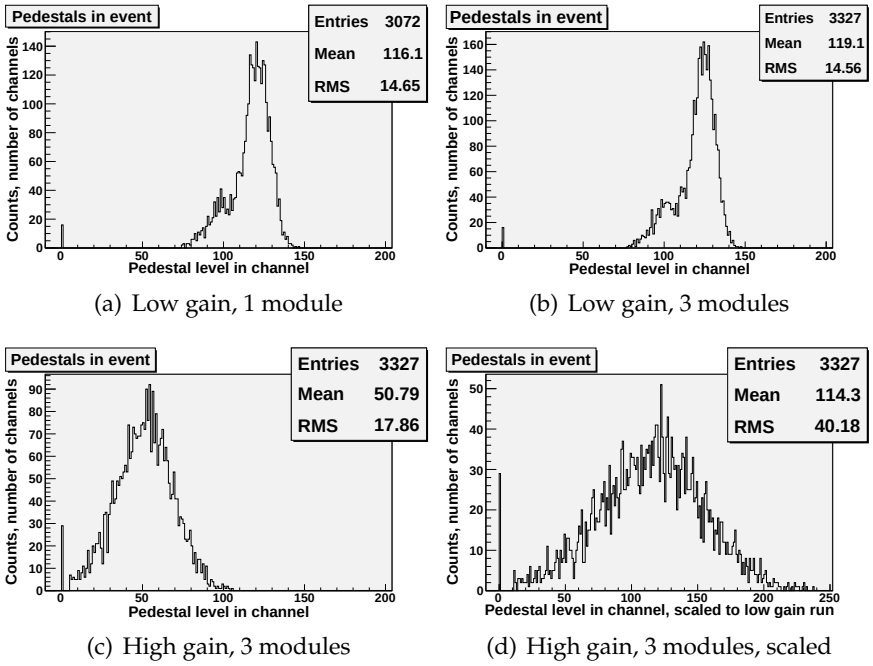

(a) Low gain, 1 module

(b) Low gain, 3 modules

(c) High gain, 3 modules

(d) High gain, 3 modules, scaled

Figure 4.20: Figures 4.20(a) - 4.20(c): Comparison of the pedestal distribution in the three different cases previously discussed (note slightly different count scales): low gain in 1 and 3 modules respectively, and high gain in 3 modules. Figure 4.20(d): The high gain event scaled to the low gain with a factor 27/12. The different shape compared to Figure 4.20(c) is due to the finer histogram resolution.

In Figure 4.20, the same comparison as for the noise levels are done for the pedestal levels of the same runs. It is clear that something changes very much at high gain (4.20(c)) compared to the low gain runs (4.20(a) and 4.20(b)). The pedestals are affected by the settings for gain, shaping time etc. in the PCA16, but also by temperature [6]. The factor 12/27 ($\approx$0.444) in amplification is also roughly seen in the ratio of the means, e.g. 50.79/116.1 ($\approx$0.437), which suggests an inverse proportionality of the pedestal level to the gain factor. This is also seen in Figure 4.20(d), which has been adjusted for the the higher gain. Here the mean falls in the same region as in the two other figures. However, the distrubution gets much broader.

Comparing the pedestal levels of the same read-out channels, for the same cabling but in different gain runs, one gets the result shown in Figure 4.21. The fewest read-out channels have precisely the same value even for noise in the gain corrected figures (4.21(b) and 4.21(d)), but the noise does not seem to change in a very systematic way. The pedestals are more spread out and are all reduced by the same factor in the high gain run compared to the low gain run. This is what has also been seen in the previous comparison (see Figure 4.20). There is a general trend in the change in pedestal levels for the different gains, and there might be a region in the noise figure which is a bit denser and has roughly the same slope as in the pedestal figure. It could indicate that the changes in the noise and pedestals are due to the same effect. Alternatively, it could just be a matter of this region (about 300 e on both axes) being where the mean is located for both distributions, as was seen in Figure 4.19. The changes in the noise are already partially explained by the digitisation effect. However, it might be that the larger spread in noise obscures any additional systematic changes.

To conclude, it seems that the FEC dependence of the noise is much weaker for a high gain

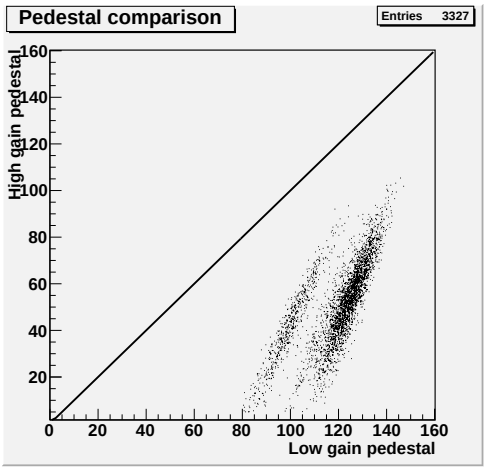

(a) Pedestals in low gain run compared to high gain run

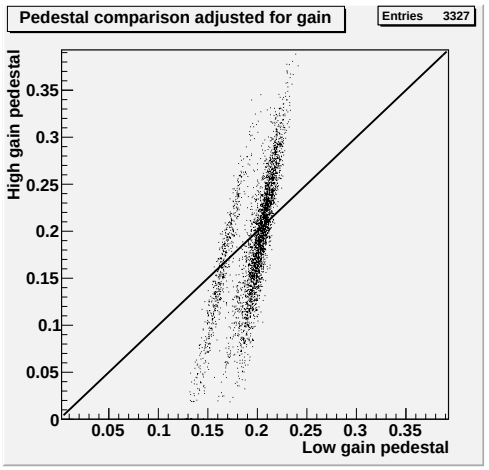

(b) Pedestals corrected for gain difference (divided by charge)

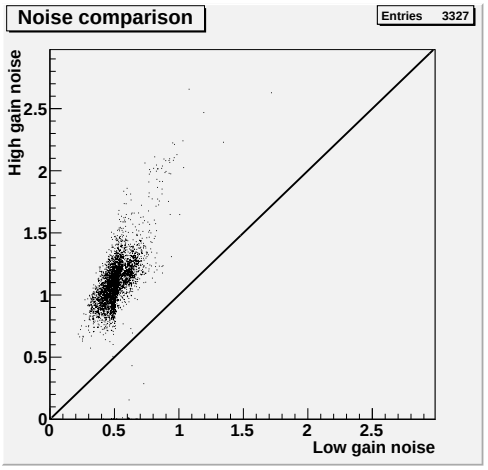

(c) Noise in low gain run compared to high gain run

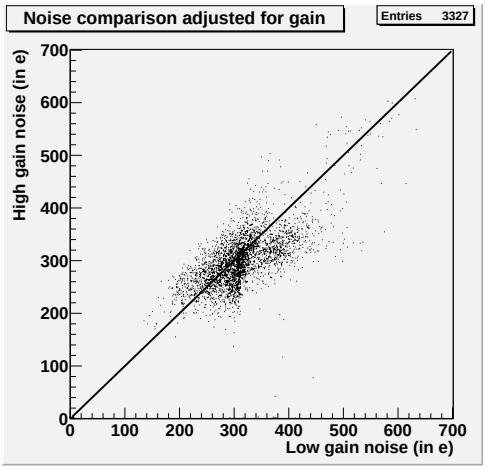

(d) Noise corrected for gain difference

Figure 4.21: Comparison of the pedestal and noise in each read-out channel at two runs with different gain. The line indicates where the levels in the different runs are equal.

run than for a low gain run. This could have at least two different interpretations. Firstly, one could imagine that any systematic effects are less visible in a situation where there is more noise. As has already been discussed, there is at least one systematic effect seen only in the low gain runs, namely the digitisation effect. However, that this should be more pronounced in low-pedestal FECs seems highly unlikely – why should lower pedestals imply analogue levels closer to the digital interval edges? The explanation is rather, in that case, that the same systematics are present, but shadowed by the more pronounced effect of the higher uncorrelated noise (as measured in ADC channels) at higher gain.

The other interpretation is that whatever affects the pedestal levels might also affect the noise. As we have seen, the noise increases with gain and the pedestals decrease. The instances in low-gain runs of low-pedestal FECs with high noise might indicate that there are FECs where the gain is higher than the set and expected value. Returning to the noise distributions in Figure 4.19, this would explain the high-noise side of the distributions of the low-gain runs,

and the entire wider spread compared to the high-gain run can thus be explained. Actually, looking at Figure 4.19(b) there seems to be a bump similar to that in Figure 4.20(b), but on the other side of the large peak. In the same way as has been done before, taking the "bump-peak-mean-to-real-peak-mean"ratios gives for the noise 380/300 ≈1.27, compared to for the pedestals 125/100=1.25. This strongly suggests that these are read-out channels with the same gain, given that the noise and pedestal dependencies on the gain are as simple as they seem (viz., proportionality and inverse proportionality). A factor 1.25 would correspond to a gain of 15 mV/fC.

From only two cases, inferring a cause is very difficult. Another possible mathematical manipulation of the distributions might for example be to displace them with a constant. Analysing more data taken at other gains would probably shed more light on the relation. Also, finding where the gain dependence sits (i.e in FEC or read-out bus position) seems helpful for finding the cause of it; for the moment, it remains unclear.

4.2.5 Influence by HV-cables

In a few of the read-out channels, the signal has periodically appearing spikes, as the one seen in Figure 4.22(a). This is thought to be an effect which emerges when the signal cables touch, or at least are affected by the field from, a high voltage cable ground braid. This situation occured in this beam test run period, as seems likely from Figure 4.22(b)). It was discussed during the run period to provide some kind of cable shielding in future tests.

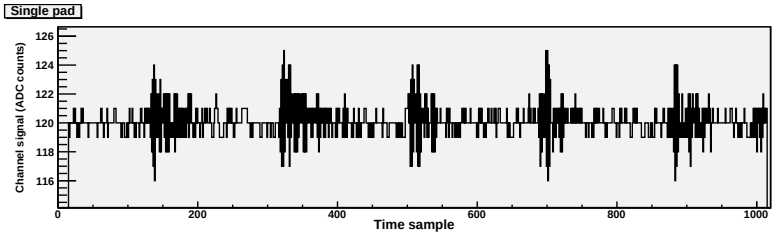

(a) Periodic spikes

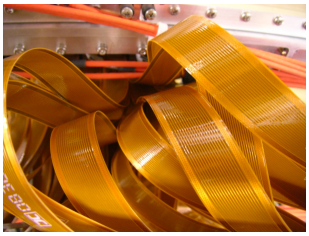

(b) Touching cables

Figure 4.22: 4.22(a): A typical spiked noise signal in one read-out channel during 1000 timesamples of a low-gain pedestal run event. This an effect of the signal cable touching a high voltage cable. 4.22(b): The signal cables connected to the central GEM module. They touch both the red high-voltage cables and each other.

4.2.6 Influence by neighbouring signal cables

Another periodicity, as the one seen in Figure 4.23, is thought to occur when signal cables cross each other. This is something which has formerly been observed [5]. This situation is also observed in Figure 4.22(b), and however rare, signal cables in the future need to be prevented from touching each other. This needs to be considered when choosing cable lengths and cable routing.

4.3 Track studies

There are two main issues considered in this analysis with respect to tracks: the collected charge in individual read-out channels and the time aspect.

The pulse shape is given by the shaper but also affected by the total charge reaching the pad. Under certain circumstances, a signal can become saturated in the amplification step, which truncates the pulse height and also affects the general shape.

The space resolution in the x-y plane has been analysed elsewhere [7]; the focus of this analysis is the resolution in the z direction, i.e. the dimension given by the signal time.

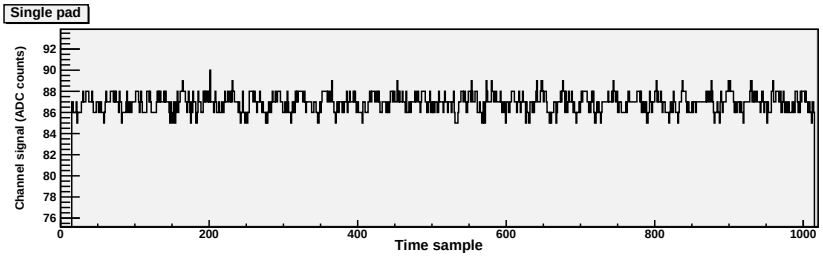

Figure 4.23: The periodicity in the signal is probably an effect of signal cables touching each other.

The tracks analysed here are only beam tracks. As it was soon discovered that there were some problems with half of the central module GEM, it was decided to temporarily skip the planned measurements at different beam angles, achieved by rotating the TPC, with only the central module instrumented. Thus, the analysed tracks are in the two 3 module cable set-ups.

It should be kept in mind that these figures contain all the raw data from an event, except for what has been rejected by the zero suppression. The tracks could be made much cleaner using software corrections such as thresholds, considering pulse arrival times etc. to filter out the noise and still not lose much "interesting" track information, but this is not in the interest of this particular analysis – rather quite the opposite.

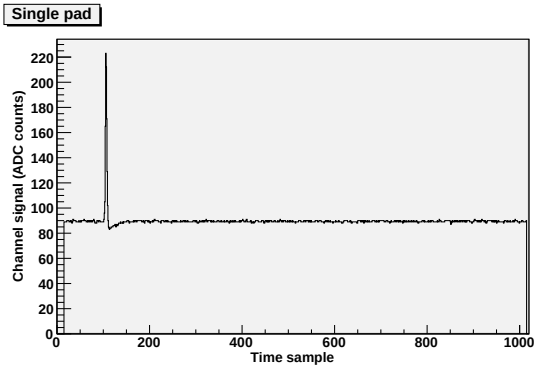

Figure 4.24: Signal without pedestal subtraction.

The signal from a read-out channel consists of a pedestal, with some noise and occasionally a pulse riding on the pedestal, as illustrated by Figure 4.24. The pedestal is normally calculated and subtracted before analysis of the data. Anything below the pedestal level will then be invisible (for example, the small inversion at the end of the pulse seen in the figure). This is in fact a consideration when choosing the direct current in the read-out channel, which gives the pedestal level. If the pedestal is too low, information might be lost below it. If it is very high, there will be less room available for representing a pulse (i.e. the ADC scale is rapidly exceeded).

The track signals used are pedestal subtracted, and typical track signals are shown in Figure 4.25. The ADC scales in these figures correspond to the colour scale when the track is drawn in two dimensions in the pad plane. One typical track in the two dimensions of the pad plane (x and y) is seen in Figure 4.26, which is a track in the first 3 module cable set-up. The track figures display the peak heights of the signals in the pads, i.e. the colour drawn corresponds to the maximum signal in the read-out channel. The beam enters from the right. The gaps

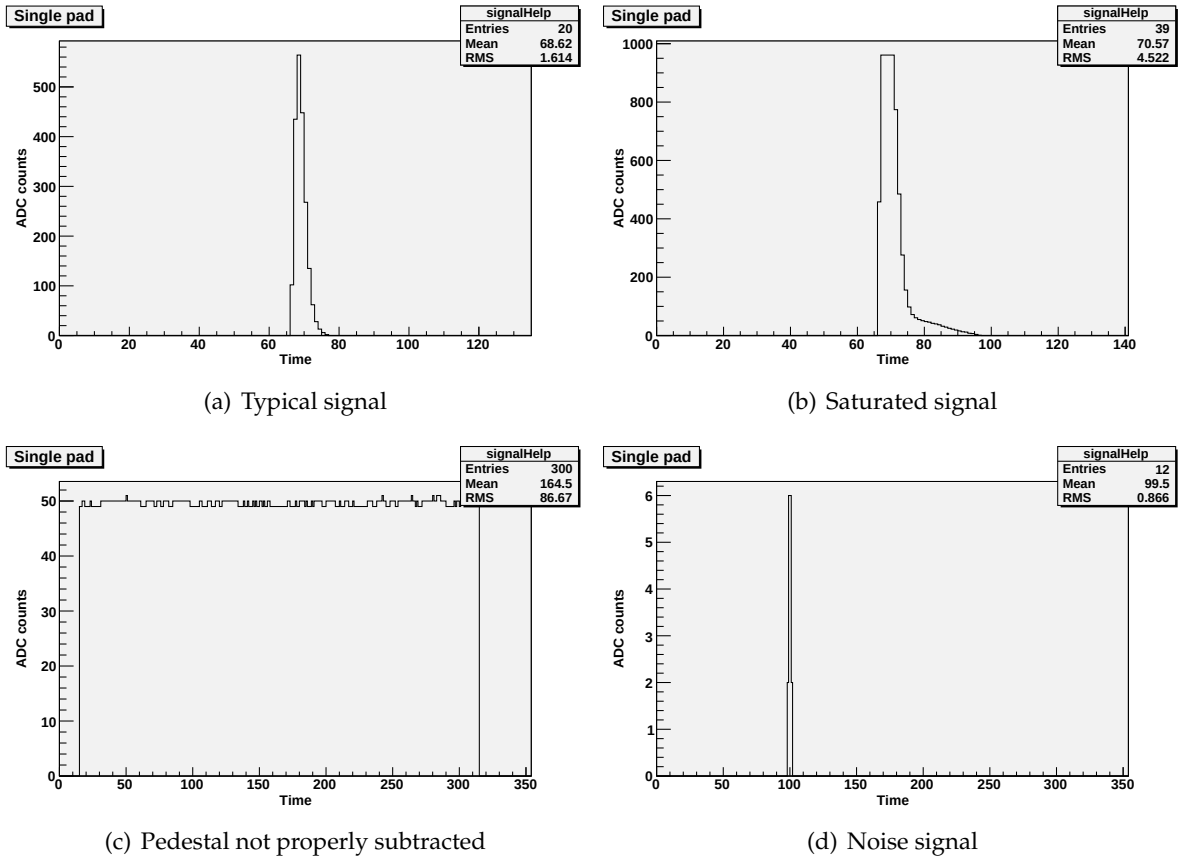

(a) Typical signal

(b) Saturated signal

(c) Pedestal not properly subtracted

(d) Noise signal

Figure 4.25: Signals in time in a selection of pads in the track shown in Figure 4.26. Note the different scales. 4.25(a): A typical signal, from the middle of the track (green pad). 4.25(b): The charge in the pad is too large to be represented by the ADC scale (high gain run event). This results in a truncation of the signal. The tail is due to saturation also in the amplifier. Red pad in the track. 4.25(c): This pad is always giving a noise signal like this, at some distance from the tracks. Violet, to the lower left in Figure 4.26. It seems that the pedestal is not correctly subtracted. 4.25(d): The signal from one of the violet pads in the area to the lower right of the track. Note the very different ADC scale from the other figures - this signal is of very low amplitude. In this figure, one clearly sees the difference in time of the violet pad pulses compared to the pads in the track.

and discontinuities in the track have three reasons: a small distance between the modules, half of the central module not being instrumented and finally mapping and module geometry representational errors. A slight curvature is seen, more easily if the global module coordinates are adjusted to make the track segments line up, and it is due to the magnetic field.

The violet pads to the lower right, which do not look like a part of the track, really are not part of the track, as can be seen from Figure 4.27: the signal in these pads arrives at another time. This violet area appears frequently in the events and runs with this cabling. They belong to cables 1 and 2 in FEC 12.

The single dot to the lower left in Figure 4.26 corresponds to the signal shown in Figure 4.25(c). It is also frequently present in the event figures.

In track events using the different instrumentations mentioned, there are often some more or less constantly firing or noisy pads to the side of the track. It might be due to some problem in the FEC (violet pads in the corner in the first 3 module cabling (see e.g. Figure 4.26) belong to FEC 12). When one looks at the other cablings, these cables do no longer as explicitly display

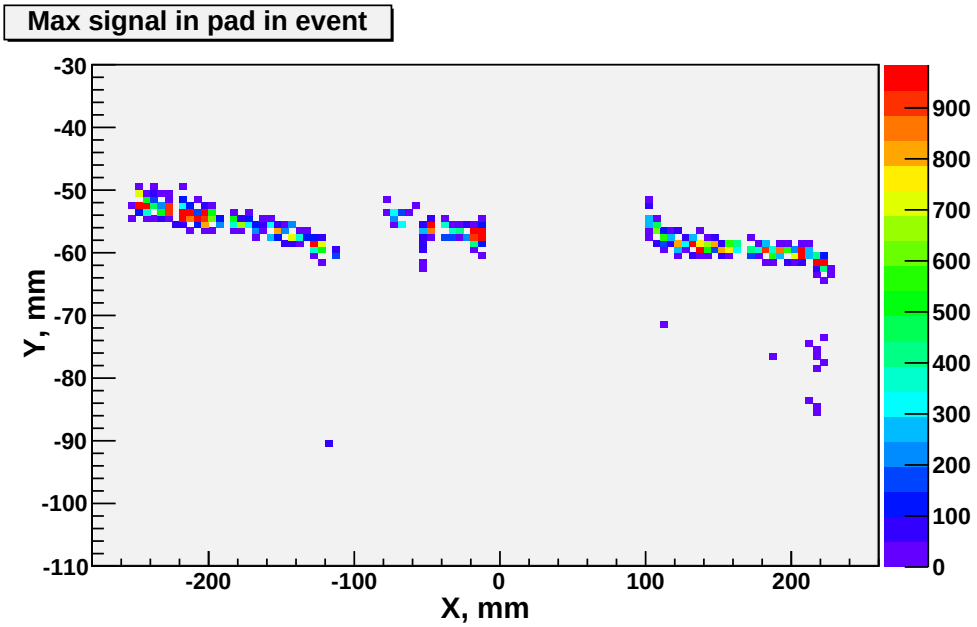

Figure 4.26: A typical track in the first 3 module cabling, B=1 T. Only half of the central module is instrumented. The colour represents the maximum charge in the read-out channel, i.e. pulse height (in most cases). Track displayed in mm, without mapping corrections.

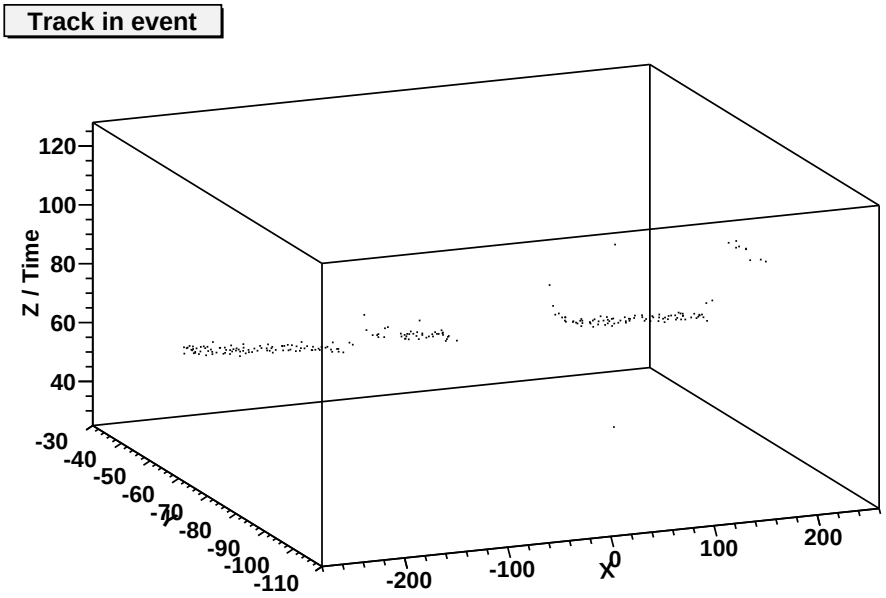

Figure 4.27: The same track as in Figure 4.26, in a 3-D representation, where the z direction is given by the timesample of the first non-zero signal in the read-out channel; z direction is given in timebins (50 ns/bin). One can see that the signal in the violet pads in Figure 4.26 arrives later than the actual track.

this behaviour, which should rule out the possibility of it being an intrinsic property of the FEC. Note that in the 1 module cabling, this FEC sits in bus position 2 and not 12 (see Figure 4.15). This suggests that it is neither a property of the position nor the FEC. As a matter of fact,

in the 1 module case, FEC 29 displays a similar behaviour, often giving a signal on the side of the track.

In some events, e.g. the one shown in Figure 4.28, there are multiple tracks. These might be due to a cosmic ray causing a signal in the time window after a trigger from the beam, or it can happen that beam particle interaction in the magnet or TPC wall creates several particles. For example, pair production by bremsstrahlung photons should be identified as two tracks bending in opposite directions, due to the opposite charges of the particles. From the relatively many occurrences of multiple tracks, it has been inferred that they indicate the beginning of an electromagnetic shower, rather than being cosmic rays [5].

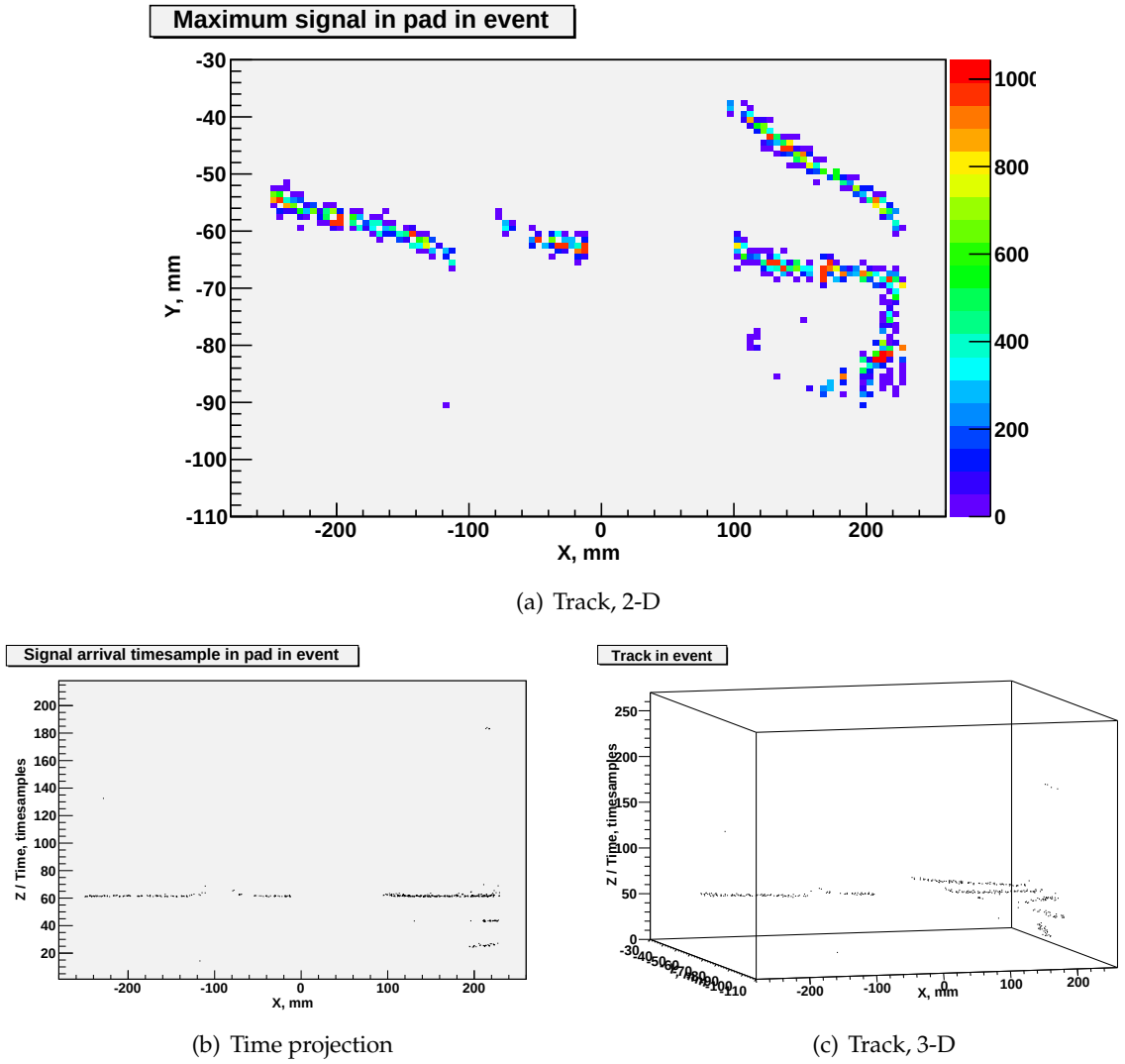

(a) Track, 2-D

(b) Time projection

(c) Track, 3-D

Figure 4.28: 4.28(a): An event with multiple tracks. The lower one is probably a delta (knock-out) electron. 4.28(b): Time projection of the same event, where one can see that not all of the tracks are simultaneous. 4.28(c): 3-D representation of the same event. The two longest (uppermost) tracks in 4.28(a) are simultaneous.

Using the later cabling, as in Figure 4.29, with the whole central module working, it is obvious that instead the leftmost (as seen in these track figures) module isn't fully operational. Another feature which is seen in this figure is certain noisy read-out channels, with a behaviour similar to what has been seen earlier in the FEC 12 cables. Here, it is not only cables on this

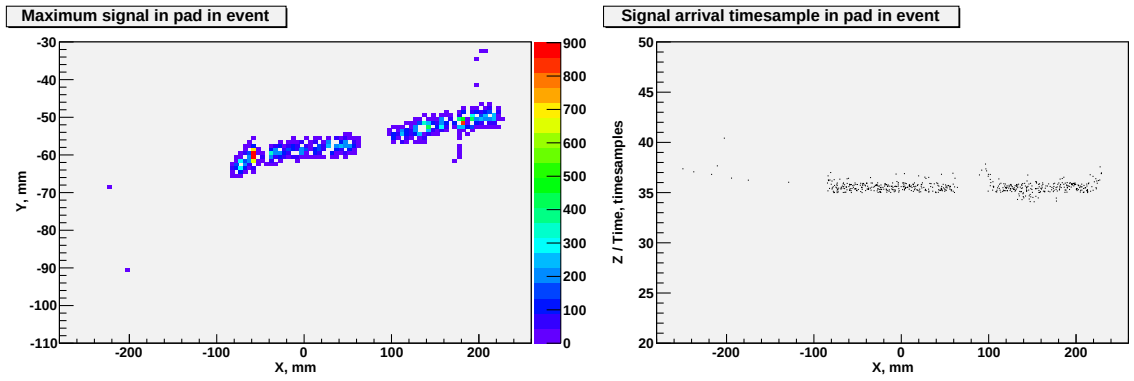

(a) Track, 2-D

(b) Track in time

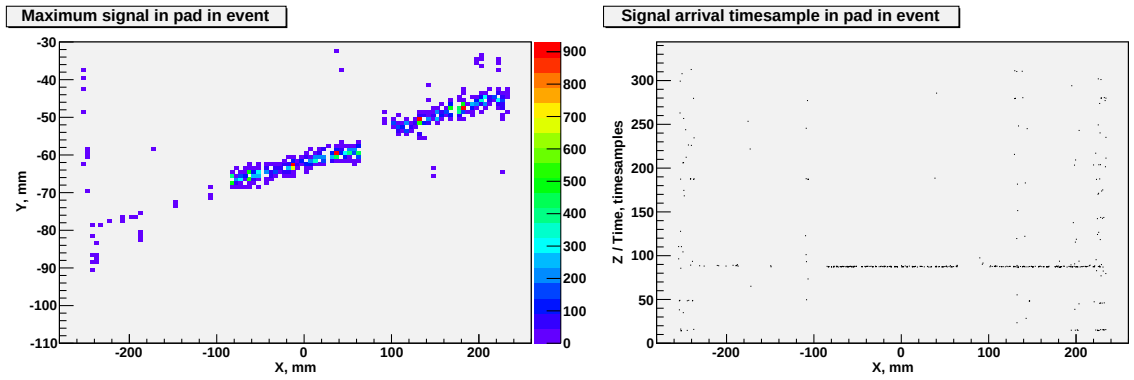

(c) Track, 2-D

(d) Track in time

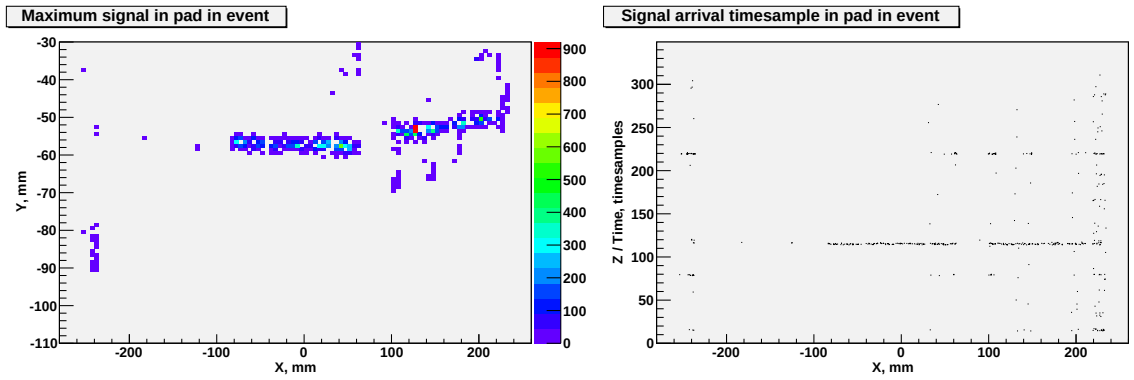

(e) Track, 2-D

(f) Track in time

Figure 4.29: Tracks in the later 3 module cabling, in a run with no magnetic field. The leftmost module as seen in the 2-D track figures seems to have a much lower GEM gain. In 4.29(b), one can see a slightly bent shape in the z direction, in the regions close to the module edges. In 4.29(c) – 4.29(f), one sees certain activated pads outside the main tracks, which display a more or less constant noise, much in the same way as has been discussed earlier (e.g. Figure 4.26).

FEC, but also on e.g. FEC 3, 6 and 31 that have this kind of noise. These read-out channels "fire" more or less all the time, be there another track closer to the beam path or not, which makes it highly improbable that this is really a track, passing instrumented areas.

If there is no connection between pads firing on the side of the track and the corresponding FEC (be it the board itself or position on the read-out bus), one could suspect that there might be some spatial effects to this: close to the module edges, there might be fields from conducting material which is not properly grounded.

Another possible explanation is that it is a cross talk effect: like a shadow of other read-out channels, the cables pick up the signal from other cables, which creates signals in them. This is however not very likely, given that the noise signal generally occurs at another (often – but not always – later) time.

It could also be an effect which emerges from these cables not being attached to the pad plane connectors. Freely hanging cables could be more prone to pick up noise (the cables work like antennas). There were really some disconnected cables in these tests, as is clearly seen in Figure 4.30; however, they should be shielded from noise from the electronics by the copper coated plates behind the FECs, and the number of entirely disconnected, freely hanging cables is comparatively small. It seems unlikely that this is the cause of the noise. Still, it would be generally desirable to have a method to determine if the pad plane end of a cable is disconnected also after completing the electronics set-up, to be able to discern these signals from those of attached cables and, if nothing else, determine if this is the cause of the noise.

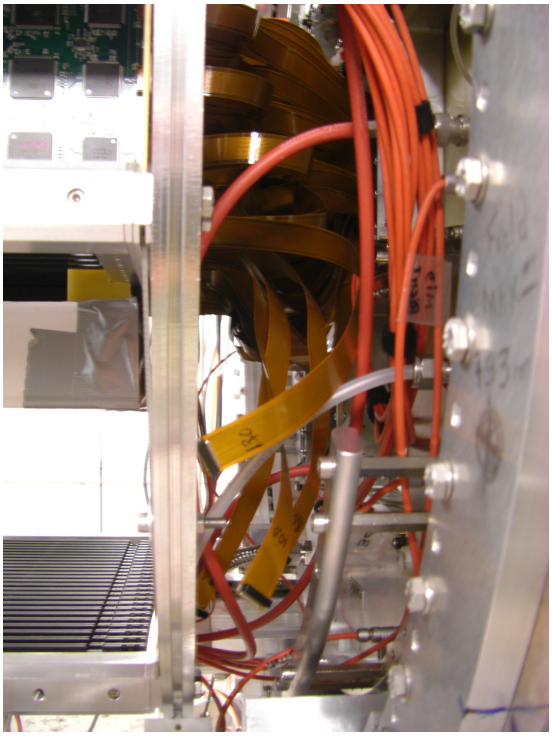

Figure 4.30: Cables that have become disconnected.

One way to prevent, to some extent, that cables detach from the connectors might be to twist the signal cables 90°. This set-up was used in the 1 module case, but in order to reach all the desired pads in the 3 module set-up, the FEC rack was rotated a quarter of a turn with

respect to the TPC, making the signals cable go untwisted from FEC to pad connector. This is probably not advantageous when it comes to distributing strain on the cable - the connectors are easily disconnected when whiggled sideways. The length of the signal cables is generally a matter to consider more. One might want to be able to e.g. instrument modules using FECs in different levels of the crate. A practical limitation of the length is however set by the problems occuring when the cables touch.

Saturated read-out channels

One thing to keep in mind when discussing time properties of the signals is the effect of saturation. Saturation means that the signal exceeds the ADC scale, but as is seen in Figure 4.25(b), the pulse shape of a saturated signal is also quite different from the others, especially if also the amplifier is saturated, giving an extra tail. In particular a saturated pulse lasts much longer than an non-saturated pulse. This affects the track width in the z direction. Choosing pedestal levels and amplification sufficiently low will decrease the number of saturated signals. Still, the level must be sufficiently high to represent what is happening in the TPC, i.e., low signals should still be visible. As a matter of fact, with the gain dependence of the pedestal level, some pedestals are close to 0 in the high gain runs (see Figure 4.21(a)). It has previously been indicated that small noise fluctuations are not properly represented at low gain, which is an indication that amplification can make a difference – even if the main point of this effect is that the noise of this detector is very low.

The number of saturated read-out channels in an event could easily be investigated further in order to optimise the pedestal levels, considering all of the above mentioned effects.

4.3.1 Absolute coordinate corrections

From the analysis by Richert, it seems that the translation from pad position in module to absolute position in space needs to be studied further, in order to match the very good position resolution obtained in these tests [7]. It might be a question of both relative translation in the y direction and rotation of the modules with respect to one another. However, since the x direction is not as much affected (since the pads are longer in this direction), this should not be a major concern in this analysis, which mainly uses the x-z plane.

4.3.2 Beam angle

A matter of interest when investigating the properties of the beam in the time dimension, i.e. z direction, is if the beam is parallel to the read-out plane. The z vs x position of charge clusters, along with a fitted line, is shown for two cases in Figure 4.31.

From a total of 10 different runs, the run with the largest angle was found to give a total deviation of about 0.8 timesamples across the entire instrumented length (about 500 mm) of the pad plane. The smallest deviation was 0.04 timesamples. From the drift velocity (see section 4.4), this amounts to a difference of 2.9 mm and 0.15 mm, respectively. (This is quite impressive; 2.9 mm in 500 mm gives a 0.3° angle.)

4.3.3 E×B field effects?

The x-y space resolution studies performed on the TPC [7] have shown a clear $\mathbf{E}\times\mathbf{B}$ field effect near the module edges. This is visible as an s-shape in these parts of the tracks. From e.g. Figure 4.29(b), there at first sight seems to be a similar effect in the x-z plane. Another possible explanation might be that charge arriving at the uninstrumented areas between the modules is collected at nearby pads at the module edges. This should only be seen as a signal arriving later in time, which actually seems to be the case from the arrival time figures of tracks (see e.g. Figures 4.28 and 4.29). However, drawing conclusions on what distorsions are causing this delayed arrival is difficult, since any deviation from the straightest path should lead to a

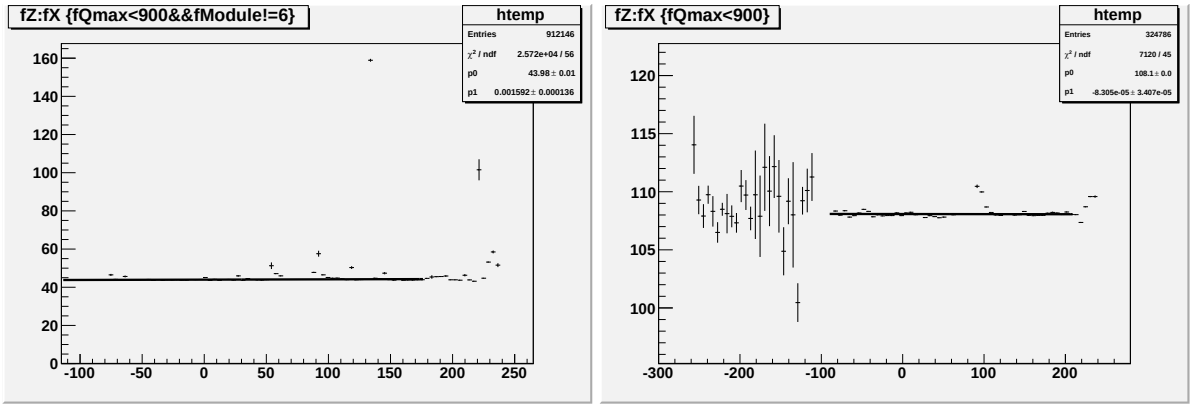

(a) Largest angle. Module 6 cut off

(b) Smallest angle. Module 6 not part of fit data set

Figure 4.31: Two examples of the fits giving the angle of the beam with respect to the pad plane. The x coordinates in mm on x axes, and z coordinates in timesamples on y axes. The data is chosen with a pad charge < 900 to avoid saturated signals, which are in general later, and with most of the edge effects cut off.

delay. Note that in these figures, it is the arrival time of the signal, i.e. first non-zero signal from the read-out channel, that is shown. This means that pulses that are extended in time due to charge arriving from neighbouring areas are not explicitly different from ordinary pulses with the same arrival time. A closer study of the individual signals from read-out channels near the edges would quite easily clarify this matter.

Another way of distinguishing the latter effect from an $\mathbf{E}\times\mathbf{B}$ field effect would simply be to compare runs with and without magnetic field with respect to this feature. In such a comparison, also distorsions due to the electric field could be more easily discernible.

4.4 Drift velocity

During the tests, the drift length in different runs has been varied, by sliding the TPC to different positions inside the magnet. Using this, one can calculate the drift velocity in the gas from the arrival time of a pulse.

At what time the pulse is seen in the read-out channel is dependent on the drift time of the electrons in the TPC, but also on the time it takes between a signal in the trigger and the response of the electronics (i.e., to "start the clock"), and on the time it takes for the beam particle to travel from the triggering scintillator system to TPC gas. The former effect is proportional to the drift length (at constant gas condititons) while all the latter will result in some constant offset.

Fitting a straight line to the data points of pulse arrival time as a function of drift length, seen in Figure 4.32, gives a drift velocity of 7.62 $\pm$0.09 cm/μs. Since the sampling frequency is 20 MHz, each timesample is 50 ns, giving a drift length of 3.8 mm/timesample. The drift time error bars in the figure are given by the standard deviation of the gaussian fit of the pulse time distribution in each run. The errors indicated on the drift length are the precision when varying the position of the TPC. It is seen that for points with multiple runs at the same distance, the different drift times are within the errors of the other run.

The offset (when extrapolated) is about 0.8 μs. For the effects influencing the offset, the electronics delays would give a negative contribution (less time will seem to have elapsed) while the tavelling time of the beam particle would give a positive contribution. The net effect here is a positive offset, and the contributing effects are not yet fully studied.

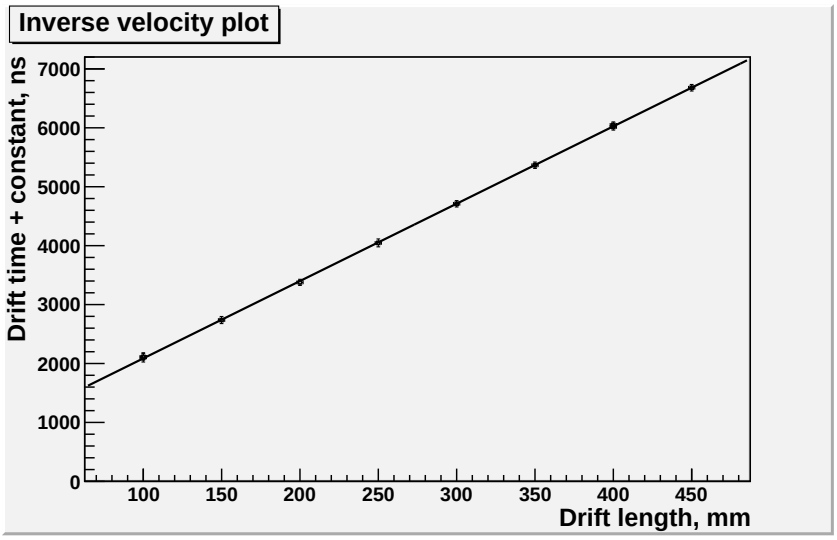

Figure 4.32: Mean of the pulse arrival time in entire runs, as a function of drift length. The pulse arrival time is the drift time plus some arbitrary offset. The points line up nicely, and the fit gives a drift velocity of 7.6 cm/μs.

4.5 Resolution in z direction

The resolution in the z direction is mainly important for the resolution of close multiple tracks and to obtain the three dimensional momentum vector. The design goal for this TPC is on the order of a few mm with respect to the two-particle separation [4].

To find the resolution in the z direction, one must first identify the charge cluster positions in the track, i.e. the position in each pad row[2] where the charge from a track reaches its maximum. Once these are found, the position in time of these signals can be found. The time position of a signal is taken to be the weighted mean of the timesamples in the pulse. These time positions should line up along a straight line, since there is no magnetic field or other effects which should bend the track in this direction. The distance from each cluster time to a fitted first-order polynomial, which will be referred to as Δz, is then a measure of the resolution. Δz for the clusters can be histogrammed and fitted by a gaussian, the standard deviation of which being a measure of the position resolution. Note that this resolution can be better than the time sample spacing. The clustering algorithm is the one used by Richert and is described elsewhere [7]. The steps used to particularly determine the resoultion in the z direction are shown in Figure 4.33 and described below.

Looking at the distribution in Figure 4.33(a), the shape seems a bit skewed. Not using the saturated pads, as in Figure 4.33(b), improves the symmetry, but not much. Drawing Δz as a function of the charge in a cluster, as in Figure 4.33(c), one sees that there is some systematic charge dependence.

Before the fit of the gaussian to the Δz peak, the dependence on the charge was corrected for. This was done by firstly not using read-out channels with maximum ADC value higher than 900 to avoid the saturated read-out channels, secondly by fitting a line to a figure of Δz vs. total charge in the cluster, and then subtracting values[3] derived from this fitted line, i.e. to some extent the charge dependence, from the Δz values.

One explanation to the charge dependence would be that the greater the charge in the pad, the more delayed the pulse becomes, since more of the tail is above the zero suppression

[2]The pads are scanned for clusters in the row direction, the direction perpendicular to the beam.

[3]a constant and a factor proportional to the cluster charge

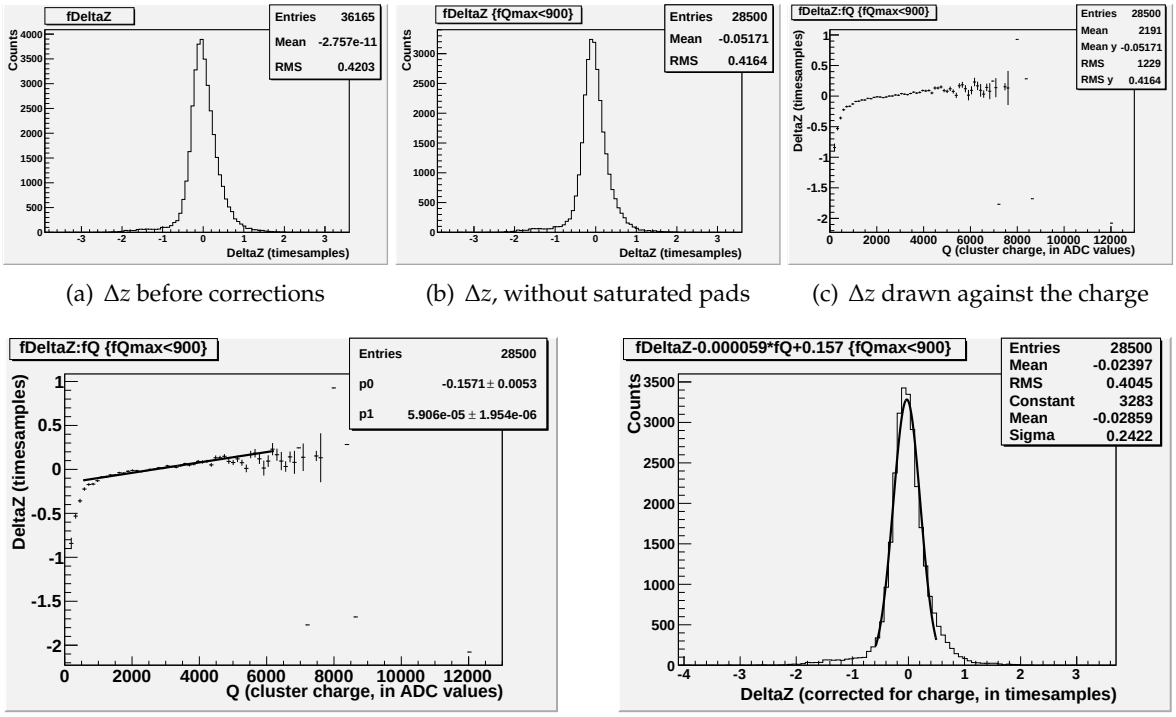

(a) Δz before corrections (b) Δz, without saturated pads (c) Δz drawn against the charge

(d) Fitted line to Δz vs charge (e) A gaussian fitted to the modified Δz

Figure 4.33: The steps in finding the resolution in the z direction.

threshold and delays the weighted mean of the time. This explanation could apply to the moderate total charges in Figures 4.33(c) and 4.33(d). For the large cluster charges, the spread in the points gets larger, but in general the pulses still arrive later than the time given by the first-order polynomial fitted to the cluster arrival times.

It should be kept in mind that, according to a delayed arrival time assumption, the clusters with the larger charge themselves most likely pull the original first order-polynomial fitted to the clusters towards a later mean, since the cluster charge effect was not compensated for in that algorithm. This could explain some of the negative arrival times.

The best results obtained using this method is a resolution of 0.217 $\pm$0.002 timesamples, corresponding to (using the drift velocity) a z direction resolution of 0.7812 $\pm$0.0072 mm. The mean result, however, is 1.5 mm for 10 runs.

4.5.1 Track width

This analysis does not cover the track width in the z direction, but there are a few aspects that are worth mentioning since they would be easily investigated.

The measured track width in the z direction should depend mainly on the drift length of the ionisation electrons and the diffusion properties of the gas. As for the diffusion properties, these might vary slightly between different runs due to the various conditions and pressure of the gas at different times, as has been mentioned before (section 3.3.2). The drift length, on the other hand, was deliberately varied, enabling analysis of the track width dependence on distance travelled by the electrons.

One feature to keep in mind is that the magnetic field doesn't affect the diffusion in the z direction (which is parallel to the field). Under the assumption that the diffusion is unaffected by the direction of the particle motion, the effect of diffusion on the path of the drift electrons

is then rotationally symmetric if there is no magnetic field at all. This implies that the width in the z direction of a track, at a given drift length, should be comparable to that in the y direction, at the same drift length, when there is no magnetic field applied (apart perhaps from resolution effects).

The distribution of charge in a cross section of the track should be that the central pads collect more charge than the periferal ones. There might be a timing-walk effect to this: since the pulse has a finite rise time, a low amplitude pulse might need longer time to reach the threshold where it is recognised as a non-zero signal, and thus it would be registered at a later time. This would clearly affect the track width in time, delaying the periferal signals. The existence of such an effect could be investigated by studying the arrival time as a function of pad centrality in the track (or, rather, in the charge cluster). As a matter of fact, already some of the figures similar to Figure 4.33(c) show a bend upwards for very low charges, indicating that pulses from low charge clusters would have a later arrival time. However, this is not what is indicated by the general charge dependence trend discussed above (section 4.5).

Chapter 5

Concluding discussion

This analysis has focused on the noise and time direction properties of the TPC prototype. The drift velocity was found to be 7.62 $\pm$0.09 cm/μs, and the z direction resolution to be 0.7812 $\pm$0.0072 mm in the best case. The GEM system seems to be a low noise system overall; however, there are a few characteristic noise effects to discuss.

First of all, there are a few noisy pads, that more or less constantly fire, on the side of the track. This effect deserves a closer look. As discussed earlier (section 4.3), this seems to be neither a distinct FEC nor read-out bus effect. This connects to some extent to the noise studies discussion of what gives the correlation between FEC and pedestal and noise levels of a read-out channel. This, however, might very well be an intrinsic FEC effect, due to some error in the gain setting of the PCA16s. It is clear that this is a matter that needs further and more systematic attention if it is to be understood.

The low noise of this TPC is clearly manifested in the digitisation effect seen in section 4.2.4, since it would not be as promininent in a system with higher noise.

It might be useful to do a Fourier transform of the signals from the pedestal runs, to get a hint as to what the noise sources might be from studying the noise frequencies involved. The electronics noise should have a certain periodicity originating from the different signal processing steps performed.

The general impression from studies of the last 3 module cabling used in the in-beam test run, which instrumented also the previously uninstrumented section of the middle module, is that these runs have more noise spread over time (see e.g. Figure 4.29).

More insight in the FEC dependencies of the noise, constantly firing pads etc. might have been gained from comparing the cabling of the second 3 module to the first. In the second one, no FECs were moved, but cables were rearranged. Different noise circumstances should emerge from this kind of action. Unfortunately, no pedestal run data were taken from this second cabling, making such a comparison very difficult. There are, however, non-zero suppressed data, from which pedestal levels etc. could be obtained, by subtracting just the pulse from each signal.

The drift velocity, diffusion constants etc. should depend on the pressure, gas content etc. inside the TPC. These parameters are given in the runlogs and can be used for finer corrections of the results, as mentioned above (see section 3.3.2).

There are a few things concerning the track width in the z direction that would be interesting to investigate further, as was already discussed in section 4.5.1. For example, writing an algorithm for offline correction of a possible timing-walk effect would improve the z resolution.

The settings for the zero suppression, such as thresholds, have not been discussed in this analysis. However, these conditions were varied during the test run, enabling a future analysis

to optimise the operation settings.

One could also investigate the influence of saturation further, on both timing properties and cluster finding, and on other information extracted from the track.

It should be very useful to complete this analysis by a wide range of simulations, to closer pinpoint detector effects and cross-check the results obtained. For example, a different sampling frequency could be simulated, which might give an insight as to what settings optimise the time resolution with respect to amount of data that needs to be handled. Already the test beam data, as it is available for short track segments in this study, provide experimental input for simulations of the expected performance of a full size TPC, which will record 2 meter track length.

Acknowledgements

I would like to thank the members of the LC-TPC collaboration, in particular those present at and involved in the in-beam test run at DESY, as well as the DESY staff. My thank yous go also to the people at the Experimental High Energy Physics Department in Lund involved in the project, especially to my supervisor Peter Christiansen for sharing his programming skills and for his many fruitful analysis suggestions. I would also like to thank Leif Jönsson and Anders Oskarsson, for insightful comments as the work has proceeded. Finally, I want to express my deeply felt gratitude towards Tuva Richert for an excellent partnership troughout this project, and for sharing her thoughts, ideas and last, but not least, her photographs.

References

1. International Linear Collider Reference Design Report,
ILC Global Design Effort and World Wide Study,
August, 2007 (available from http://www.linearcollider.org at August 13, 2009)

2. ALICE Collaboration,
Time Projection Chamber,
ALICE TDR 7, CERN/LHCC 2000-001.

3. D. Antończyk et al.,
Nuclear Instruments and Methods in Physics Research A565 (2006), 551-560

4. Leif Jönsson,
Experimental High Energy Physics, Lund University
Private communication, February-August 2009

5. Anders Oskarsson,
Experimental High Energy Physics, Lund University
Private communication, February-August 2009

6. Ulf Mjörnmark,
Experimental High Energy Physics, Lund University
Private communication, August 2009

7. T. Richert,
Analysis of the Gas Electron Multiplier Read Out System for the International Linear Collider Time Projection Chamber Prototype,
Bachelor's Dissertation, Lund University, 2009

Pictures:

8. ILC web page, http://www.linearcollider.org,
August 13, 2009

9. CERN Gas Detector Development Group web page, http://gdd.web.cern.ch/GDD/,
August 18, 2009

10. Hirotoshi Kuroiwa,
Saga University, Japan
Private communication, February 19, 2009

All photographs courtesy of Tuva Richert